

A single-cell transcriptomic atlas reveals resident dendritic-like cells in the zebrafish brain parenchyma

Reviewed Preprint

Published from the original preprint after peer review and assessment by eLife.

[About eLife's process](#)

Reviewed preprint version 1

January 9, 2024 (this version)

Sent for peer review

September 29, 2023

Posted to preprint server

July 28, 2023

Mireia Rovira, Giuliano Ferrero, Magali Miserocchi, Alice Montanari, Valérie Wittamer 

Institut de Recherche Interdisciplinaire en Biologie Humaine et Moléculaire (IRIBHM) • ULB Institute of Neuroscience (UNI), Université Libre de Bruxelles (ULB), Brussels, Belgium

 https://en.wikipedia.org/wiki/Open_access

 Copyright information

Abstract

Recent studies have highlighted the heterogeneity of the immune cell compartment within the steady-state murine and human CNS. However it is not known whether this diversity is conserved among non mammalian vertebrates, especially in the zebrafish, a model system with increasing translational value. Here, we reveal the complexity of the immune landscape of the adult zebrafish brain. Using single-cell transcriptomics, we characterized these different immune cell subpopulations, including cell types that have not been -or have been poorly-characterized in zebrafish so far. By histology, we found that, despite microglia being the main immune cell type in the parenchyma, the zebrafish brain is also populated by a distinct myeloid population that shares a gene signature with mammalian dendritic cells (DC). Notably, zebrafish DC-like cells rely on *batf3*, a gene essential for the development of conventional DC1 in the mouse. Using specific fluorescent reporter lines that allowed us to reliably discriminate DC-like cells from microglia, we quantified brain myeloid cell defects in commonly used *irf8*^{-/-}, *csf1ra*^{-/-} and *csf1rb*^{-/-} mutant fish, revealing previously unappreciated distinct microglia and DC-like phenotypes. Overall, our results suggest a conserved heterogeneity of brain immune cells across vertebrate evolution and also highlights zebrafish-specific brain immunity characteristics.

eLife assessment

This **important** work reports on the transcriptomic analysis of leukocytes in the brain of adult zebrafish. A specific novel finding is the identification of dendritic cells distinct from microglia or macrophages; regional distribution of these subsets is described using transgenic lines and immunohistochemistry. The dependence of these subsets of specific transcription factors or receptors is addressed with mutants. This is a thorough and **compelling** analysis, of interest for scientists using the zebrafish models for neurology, immunology, and infectiology, as well as for those interested in the evolution of the brain and immune system.

Introduction

Over the last years, several landmark studies leveraging high-dimensional techniques have contributed to uncovering the cellular complexity of the human and murine central nervous system (CNS) immune landscapes (Mrdjen et al. 2018 [↗](#); Hammond et al. 2018 [↗](#); Masuda et al. 2019 [↗](#); Van Hove et al. 2019 [↗](#); Jordao et al. 2019 [↗](#); Bottcher et al. 2019 [↗](#)). From these works, it was found that, besides parenchymal microglia, the steady-state CNS also harbors diverse leukocytes localized at the CNS-periphery interfaces, including different subtypes of mononuclear phagocytes (MNPs) such as border-associated macrophages (BAMs), monocytes and dendritic cells (DCs)-, along with lymphocytes (T cells, B cells, NK cells or innate lymphoid cells ILCs) and granulocytes (neutrophils). Several of these immune cell populations have since been shown to play important roles in regulating CNS development and homeostasis (Drieu et al. 2022 [↗](#); Pasciuto et al. 2020 [↗](#); Tanabe and Yamashita 2018 [↗](#)), or identified as key players in disease models and aging (Alves de Lima et al. 2020 [↗](#); Minhas et al. 2021 [↗](#)). Collectively, these studies have highlighted how understanding vertebrate brain leukocyte heterogeneity is key to describe CNS interactions with the microenvironment and other cells such as glial cells, neurons or endothelial cells. In contrast, the CNS immune cell repertoire of other vertebrate models is poorly defined.

This is the case for the zebrafish, an increasingly recognized model for translational research on human neurological diseases, owing to its strong genetics and conserved physiology with mammals (Turrini et al. 2023 [↗](#); Liu 2023 [↗](#); D'Amora et al. 2023 [↗](#)). Over the years, the zebrafish has also gained considerable importance in regenerative research due to its remarkable capacities for organ regeneration, including the CNS. While this model has contributed to elucidate important cellular and molecular mechanisms underlying adult brain regeneration (Kizil et al. 2012 [↗](#); Zambusi et al. 2022 [↗](#); Saraswathy et al. 2022 [↗](#)), much of the work has largely focused on the neurogenesis side of the equation. However, as it is becoming increasingly clear that inflammation plays key roles in the regeneration process (Kyritsis et al. 2012 [↗](#)), attention has recently shifted to non-neuronal brain cell types, especially immune cells. While microglia in the zebrafish adult brain have been identified and characterized in bulk RNAseq studies (Oosterhof et al. 2018 [↗](#); Ferrero et al. 2018 [↗](#); Ferrero et al. 2021 [↗](#); Wu et al. 2020 [↗](#)), the phenotypic heterogeneity within the microglial compartment remains unknown. In addition, a complete description of all immune cell populations present in the adult zebrafish brain at steady-state is currently lacking. This is a precondition for studying the complex cellular orchestration that takes place in the healthy and diseased CNS. In an effort to understand the cellular basis of the immune compartment of the zebrafish brain, we have established reliable protocols for dissociation and prospective isolation of brain leukocytes, using fluorescent transgenic lines. By combining this approach with single-cell RNA sequencing, we have generated a gene expression atlas composed of the distinct immune cells present in the homeostatic brain. This dataset revealed the presence of subpopulations of mononuclear phagocytes and other leukocytes, including cell types that have not been -or have been poorly-characterized so far. Here, we present the characterization of a new mononuclear phagocyte population that represents an important fraction among all brain leukocytes and coexist with microglia in the brain parenchyma. This population of cells is *batf3*-dependent and expresses known DC canonical genes. In light of these observations, we have also revisited the phenotype of myeloid-deficient mutant lines, such as *csf1ra*^{-/-}, *csf1rb*^{-/-} and *irf8*^{-/-} fish, that have been instrumental to the field. Overall, we provide an overview of the immune landscape in the adult zebrafish brain which, akin to findings in mammals, boasts distinct myeloid and lymphoid cell types.

Results

Mononuclear phagocytes represent the main immune cell population in the adult zebrafish brain

As a first step, we sought to assess the leukocytes present in the zebrafish adult brain according to their cellular morphology. We previously showed the *cd45:DsRed* transgene labels all leukocytes, with the exception of B lymphocytes (Wittamer et al. 2011 [↗](#); Ferrero et al. 2020 [↗](#)). Therefore, we performed May-Grünwald Giemsa (MGG) staining on a pure population of *cd45:DsRed*⁺ cells isolated from the brain of adult *Tg(cd45:DsRed)* transgenic animals by flow cytometry (Figure 1A [↗](#)). Cells with the classical morphological features of mononuclear phagocytes were identified as macrophages/microglia based on their large and vacuolated cytoplasm (Wittamer et al. 2011 [↗](#)) (Figure 1B [↗](#)). Monocytes, recognized by their kidney-shaped nuclei, were also present, as well as cells with a typical dendritic cell morphology, namely elongated shapes, large dendrites and oval or kidney-shaped nuclei (Lugo-Villarino et al. 2010 [↗](#)) (Figure 1B [↗](#)). We also found large numbers of lymphocytes, clearly distinguished from myeloid cells by their smaller size and narrow and basophilic cytoplasm stained in blue. The remaining cells were neutrophils, characterized by their clear cytoplasm and highly segmented nuclei.

Next, we took advantage of fluorescent zebrafish transgenic lines, allowing to detect and quantify the different leukocyte subsets using flow cytometry. To achieve this, *Tg(cd45:DsRed)* animals were crossed to established GFP reporters that label mononuclear phagocytes (*Tg(mpeg1:GFP)*), neutrophils (*Tg(mpx:GFP)*), NK and T lymphocytes (*Tg(lck:GFP)*) or IgM-expressing B cells (*Tg(ighm:GFP)*) (Figure 1A [↗](#)). As expected, flow cytometry analyses of these double transgenic fish demonstrated that *mpeg1:GFP*⁺ mononuclear phagocytes were the most abundant leukocytes in the adult brain, accounting for $75.7\% \pm 2.9$ of the total *cd45:DsRed*⁺ population (n=4) (Figure 1C,D [↗](#)). In contrast, *mpx:GFP*⁺ neutrophils were scarce, representing only $0.2\% \pm 0.04$ of brain leukocytes (n=4) (Figure 1-supplement 1A). Regarding lymphocytes, *lck:GFP*⁺ NK/ T cells were more abundant than *ighm:GFP*⁺ B cells, accounting for $7.2\% \pm 0.9$ (n=4) and $0.2\% \pm 0.01$ (n=4), respectively (Figure 1-supplement 1B,C).

Although *mpeg1*-driven fluorescent transgenes are commonly used to label mononuclear phagocytes, we and others have previously shown that *ighm*-expressing B cells are also marked by these reporters, as they endogenously express *mpeg1.1* (Ferrero et al. 2020 [↗](#); Moysé and Richardson 2020 [↗](#)). However, based on the low numbers of brain *ighm:GFP*⁺ cells identified in our flow cytometry analyses, we concluded their contribution to the *mpeg1*⁺ population was minimal and that brain *mpeg1*⁺ cells mostly comprise mononuclear phagocytes. We thus wondered what was the specific proportion of microglial cells within the *mpeg1*⁺ population. To address this question, we crossed *Tg(cd45:DsRed)* fish to animals carrying the *Tg(p2ry12:p2ry12-GFP)* transgene (Sieger et al. 2012 [↗](#)). P2ry12 is an evolutionary conserved canonical microglia marker, including in zebrafish (Mazzolini et al. 2019 [↗](#); Rovira et al. 2022 [↗](#); Ferrero et al. 2018 [↗](#)), so its expression can serve to discriminate microglia from other brain macrophages, as shown previously in mammals (Butovsky et al. 2014 [↗](#)). Interestingly, analyses of brain cell suspensions from double transgenics showed *p2ry12:GFP*⁺ microglia accounted for half of *cd45:DsRed*⁺ cells ($50.9\% \pm 2.9$; n=4) (Figure 1D,E [↗](#)). Considering that *mpeg1:GFP*⁺ cells comprised ~75% of all leukocytes, these results indicated that approximately 25% of brain mononuclear phagocytes do not express the microglial *p2ry12:GFP*⁺ transgene. Based on our cytological observations, this population likely contains a mixture of monocytes and dendritic cells. Collectively, these analyses suggest an important diversity among leukocytes present in the steady-state brain of the adult zebrafish.

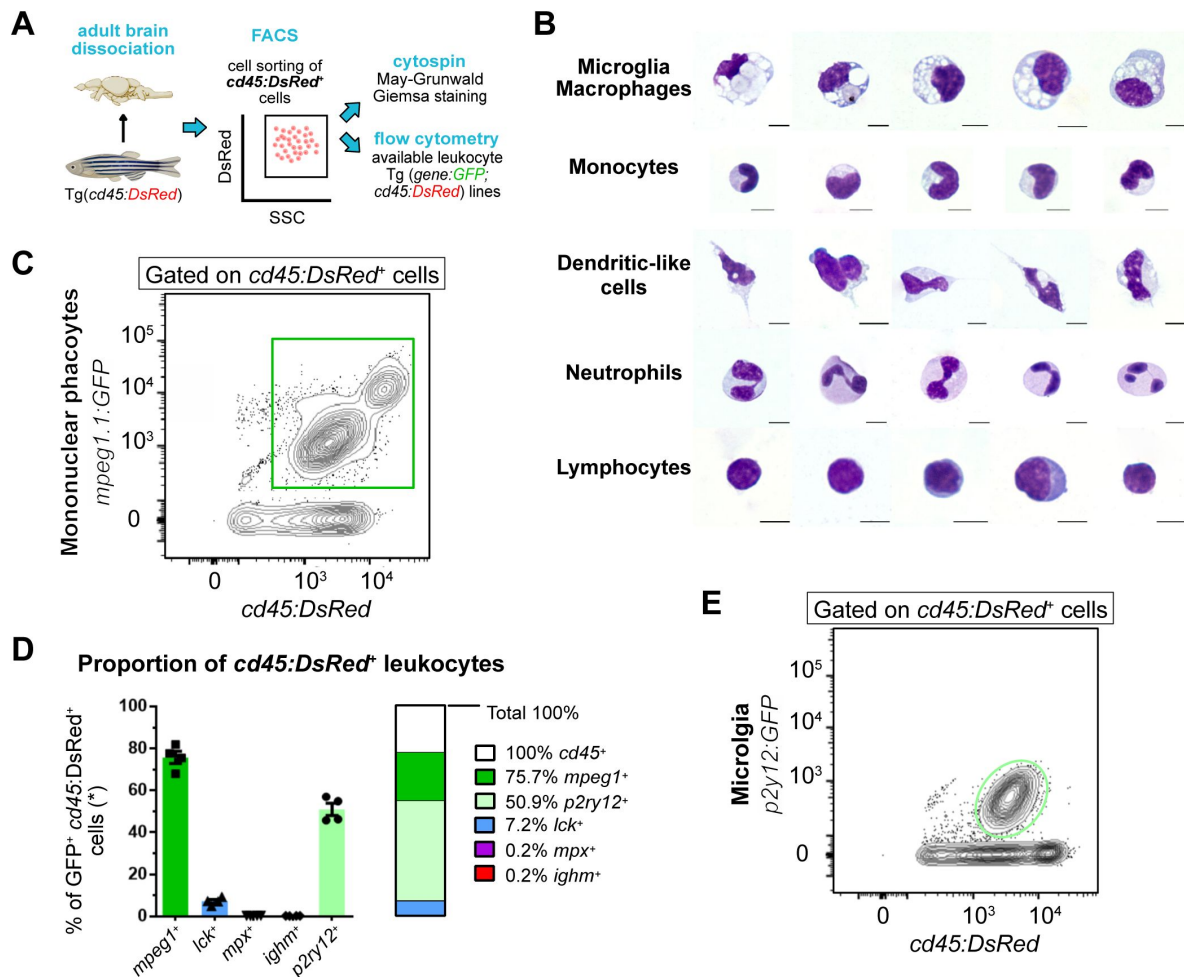


Figure 1.

Leukocyte heterogeneity in the adult zebrafish brain using blood lineage-specific transgenic lines.

A. Schematic overview of the experiment. First, *cd45:DsRed*⁺ cells were sorted, cytopspined and stained with May-Grunwald Giemsa (MGG). In parallel, lines carrying the *cd45:DsRed* transgene in combination with blood lineage-specific GFP reporters were analyzed by flow cytometry. **B.** Morphology of brain-sorted *cd45:DsRed*⁺ cells stained with MGG. Microglia and/or macrophages, monocytes, dendritic cells, neutrophils and lymphocytes were identified. The scale bar represents 5 μ m. **C.** Flow cytometry analysis on brain cell suspensions from adult Tg(*mpeg1:GFP; cd45:DsRed*) identifying *mpeg1:GFP*⁺; *cd45:DsRed*⁺ mononuclear phagocytes (green gate). **D.** Proportion of brain immune cell types, as determined by flow cytometry analysis on cell suspensions from fish carrying *cd45:DsRed*⁺ and a lineage-specific GFP reporter ($n=4$ fish). The percentage relative to total *cd45:DsRed*⁺ leukocytes is shown, with the exception of Tg(*ighm:GFP; cd45:DsRed*) which are not normalized as the *cd45:DsRed* transgene is not expressed in the B cell lineage. **E.** Flow cytometry analysis of brain cell suspensions from an adult Tg(*p2ry12:p2ry12-GFP; cd45:DsRed*) fish, identifying *p2ry12:p2ry12-GFP*⁺; *cd45:DsRed*⁺ microglial cells (light green gate). n refers to the number of biological replicates. Data in (D) are mean \pm SEM.

Single-cell transcriptomics identifies multiple leukocyte populations in the adult brain

To fully characterize the heterogeneity within the zebrafish brain immune landscape, next we turned to single-cell transcriptome profiling. Viable *cd45:DsRed*⁺ cells were FACS-sorted from the steady-state brain of adult *Tg(cd45:DsRed)* animals, then subjected to scRNA-sequencing using the 10X platform (Figure 2A, Appendix 1-Figure 2). After an unsupervised uniform manifold approximation and projection (UMAP) and single-cell clustering, we obtained a total of 20 cell clusters (Figure 2B). A preliminary observation of our dataset, revealed the expression of *cd45* (also known as *ptprc*) in all clusters of the dataset, thus confirming their hematopoietic identity (Figure 2C). In addition, expression of canonical genes for mononuclear phagocytes (*mpeg1.1*), neutrophils (*mpx*) or T/ NK cells (*lck*, *lymphocyte-specific protein tyrosine kinase*) were found in several clusters (Figure 2C). Together, these initial observations indicated that we were able to capture a repertoire of different brain leukocytes represented in individual cluster identities. This is in line with the cell type diversity determined from our cytological and flow cytometry analyses.

Cluster annotation was achieved based on expression of defined blood lineage-specific genes previously established in zebrafish (Tang et al. 2017; Hernández 2018; Moore et al. 2016), and from published transcriptomes from human and mouse brain leukocytes (Mrdjen et al. 2018; Jordao et al. 2019; Hammond et al. 2018; Masuda et al. 2019; Van Hove et al. 2019). Using these approaches, we were able to annotate 15 clusters. The remaining cells are included in the online material but were not used for further analysis in this study. We identified 7 major leukocyte populations that comprised microglia (MG), macrophages (MF), dendritic-like cells (DC-like), T cells, natural killer cells (NK), innate lymphoid-like cells (ILCs) and neutrophils (Neutro) (Figure 2B, Table 1). Expression of the markers for each cluster is visualized plotting the top 50 marker genes (Figure 2D and Table 2). Of note, one cluster was annotated as proliferative (Prolif) because of the expression of proliferative markers, suggesting the presence of dividing brain leukocytes, however, marker genes were not indicative of a specific cell type (Figure 2 B,D and Table 1). A detailed analysis of the different clusters from the lymphoid and myeloid compartments is presented in the following sections, with an emphasis on microglia and DC-like clusters.

The adult zebrafish brain contains innate and adaptive lymphoid cells

Expression of *lck*, a conserved marker for T lymphocytes and NK cells (Moore et al. 2016), identified three clusters of lymphoid cells (Figure 2C, Table 1). Two of them expressed T cell-specific marker genes such as *zap70* (tcr-associated protein kinase), TCR co-receptors including *cd4-1*, *cd8a*, *cd8b* and *cd28*, and *il7r*, a cytokine receptor that functions in T cell homeostasis (Figure 3A,D), all of them showing conservation between mammals and zebrafish. This suggests that these two *zap70*-expressing clusters contain a mix of CD4⁺ and CD8⁺ T cells, and were thus annotated as Tcells1 and Tcells2. Interestingly, a proportion of cells within these clusters expressed *runx3*, which in mammals has been reported as a regulator of tissue resident memory CD8 T cells in different tissues, including the brain (Milner et al. 2017). The second cluster highly expressed genes previously described as markers for NK cells in the zebrafish whole kidney marrow (WKM) (Tang et al. 2017; Carmona et al. 2017), such as chemokines *ccl36.1* and *ccl38.6*, granzymes *gzm3.2* and *gzm3.3*, *il2rb* and *ifng1* (Figure 3B,D). However, expression of novel immune-type receptor (*nitr*) or NK-lysin genes was not detected in brain NK cells, in contrast to WKM NK cells (Carmona et al. 2017; Moore et al. 2016; Yoder et al. 2010). Annotation of these lymphoid clusters was mostly based on a zebrafish WKM reference data set (Tang et al. 2017) and therefore, differences may exist between tissues.

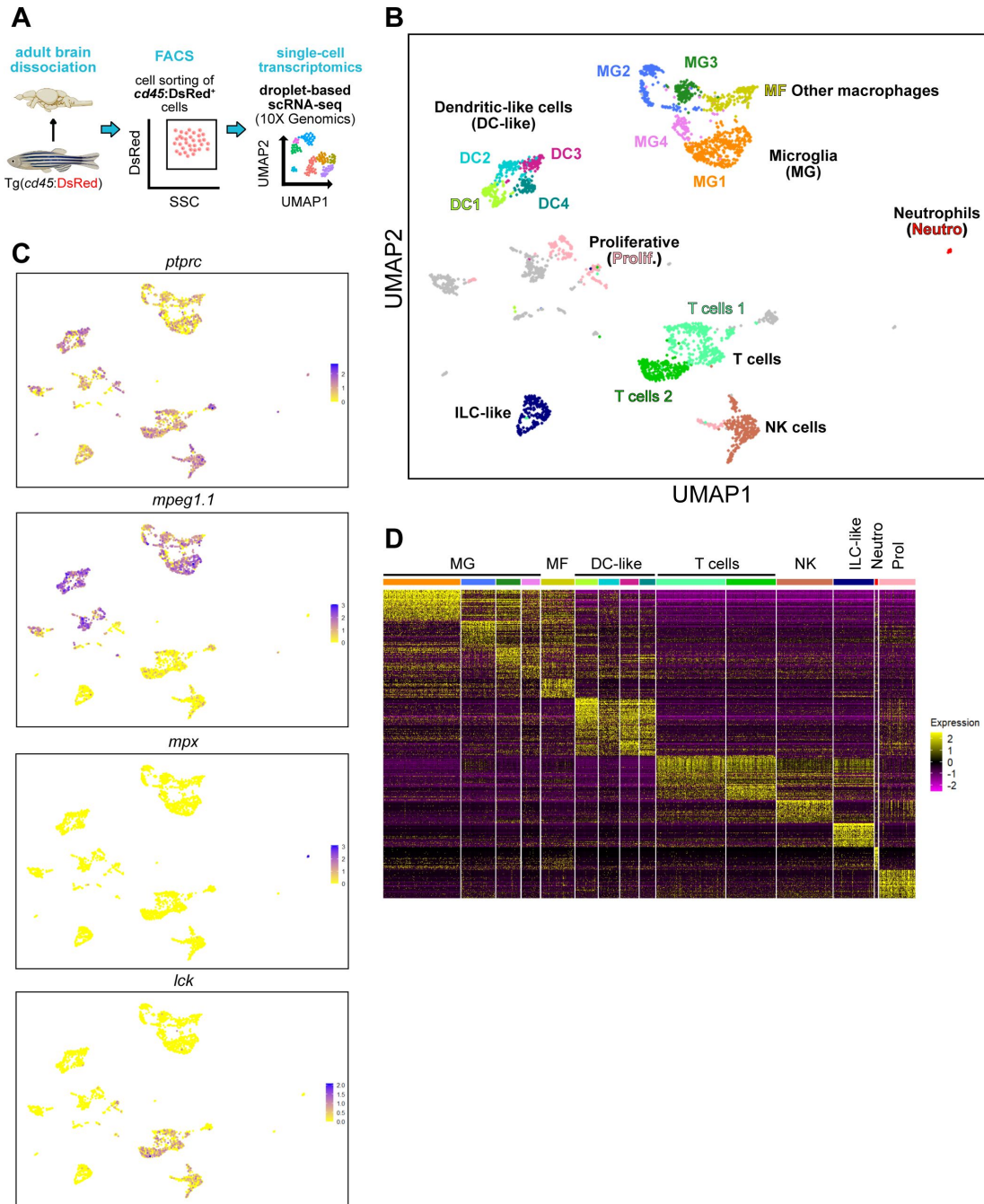


Figure 2.

Diversity of brain leukocytes as shown by single-cell transcriptomics.

A. Schematic overview of the experimental approach. Single-cell profiling of total brain *cd45:DsRed*⁺ leukocytes (pool from 3 individual fish) was performed using the 10X Genomics platform. **B.** Split Uniform Manifold Approximation Projection (UMAP) of brain *cd45:DsRed*⁺ cells with annotated cell populations. Clusters in grey shade are not indicative of a specific cell type and were not annotated. **C.** UMAP plots depicting the expression pattern of *ptprc*, also known as *cd45* (leukocytes), *mpeg1.1* (mononuclear phagocytes), *mpx* (neutrophils) and *lck* (T and NK lymphocytes). Gene expression levels from low to high are indicated by a color gradient from yellow to purple (normalized counts in log₁p). **D.** Heat map of the top differentially up-regulated genes in each cluster (row=gene, column=cell type). Color scale (gradual from purple to yellow) indicates the expression level (average log₂ fold change).

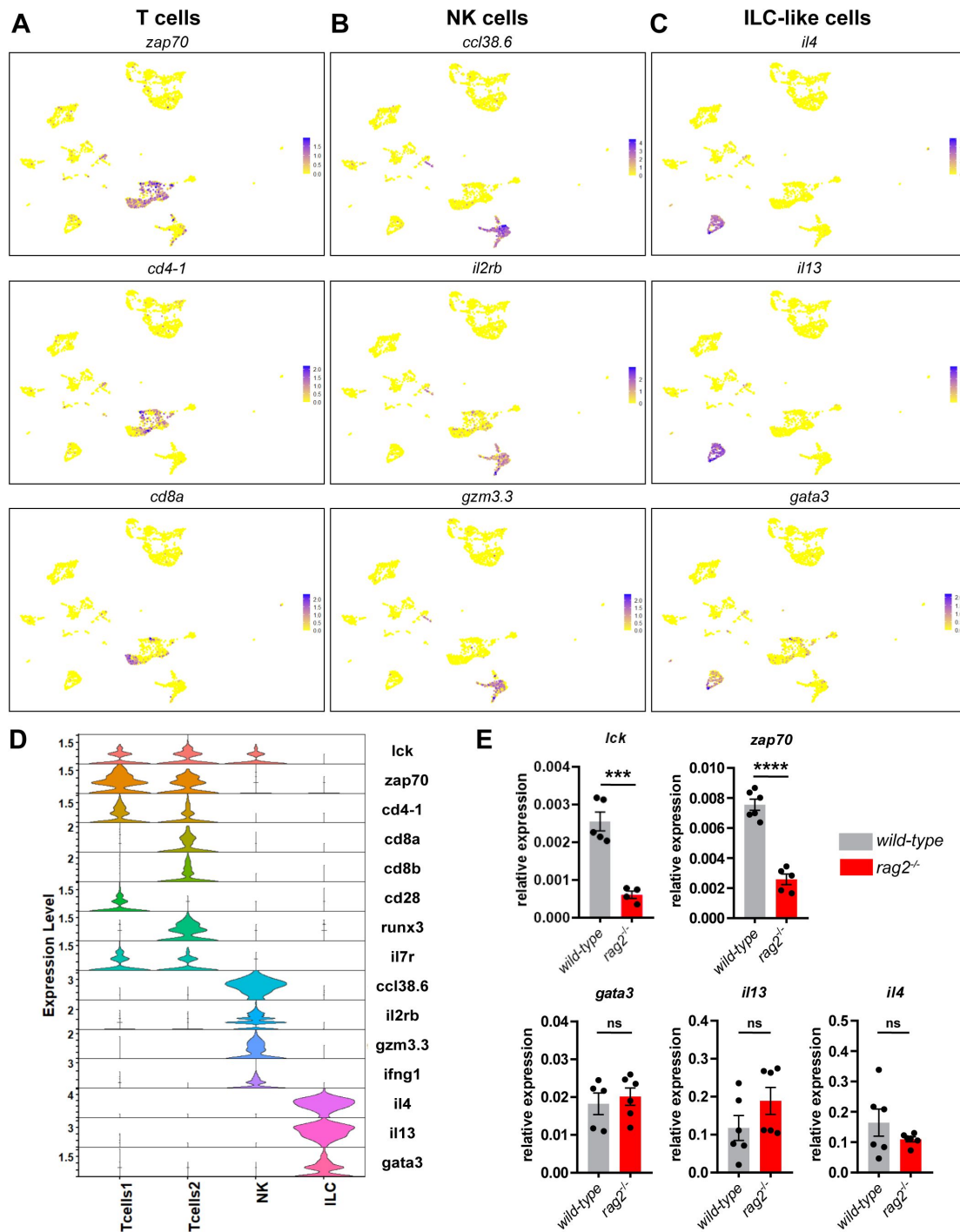


Figure 3.

Single-cell RNA sequencing identifies several lymphocyte subpopulations in the adult brain.

A-C. UMAP visualization of the expression of selected genes in the annotated T cell clusters Tcells1 and Tcells2 (*zap70*, *cd4-1* and *cd8a*), NK cluster (*cc138.6*, *il2rb*, *gzm3.3*) and ILC-like cluster (*il4*, *il13* and *gata3*). Color scale (gradual from yellow to purple) indicates the expression level for each gene (normalized counts in log₁p). **D.** Violin plots representing the expression levels of known lymphocyte markers (normalized counts in log₁p) within the different clusters. **E.** Comparison of the relative expression of *lck*, *zap70*, *gata3*, *il13* and *il4* transcripts between brain *cd45:DsRed*⁺ cells isolated by FACS from T cell-deficient *rag2*^{-/-} mutants (red bars) and their *wild-type* siblings (grey bars). Each data point represents an individual fish (*n*=6) and error bars indicate SEM. *** *P*<0.001, **** *P*<0.0001 (Two-tailed unpaired t-test).

Notably, we identified an additional cluster that did not express any of the previously mentioned T cell markers but displayed *il4* and *il13* expression in a large proportion of cells (**Figure 3C,D**). In mammals, these two cytokines identify CD4⁺ T helper type 2 cells as well as innate-lymphoid cells type 2 (ILC2s), the innate counterparts of adaptive T helper cells (Vivier et al. 2018). Interestingly, this cluster was also positive for *gata3*, a transcription factor that regulates the development and functions of ILC2s (Wong et al. 2012). The expression profile identified in this cluster may thus represent the molecular signature of zebrafish ILC2-like cells (Vivier et al. 2016). To test this hypothesis, we performed qPCR analyses on *cd45:DsRed*⁺ brain cells isolated from *rag2*-deficient fish. We hypothesized that, like their murine counterparts (Spits and Cupedo 2012), *rag2* mutant zebrafish, which lack T and B cells (Tang et al. 2014), would still produce ILC-like cells. Supporting this postulate, while the expression levels of *lck* and *zap70* was significantly reduced in brain leukocytes from the *rag2* mutants in comparison with that from their *wild-type* siblings (**Figure 3E**), *gata3*, *il4* and *il13* showed similar expression levels between cells from both genotypes (**Figure 3E**). It thus appears that the expression of putative ILC2 cell-associated genes in brain leukocytes is not changed in the absence of T cells. Altogether, these findings support our annotation of this cluster as ILC-like cells.

The adult brain contains other *mpeg1*-expressing cells beside microglia

As shown in **Figure 2C**, expression of *mpeg1.1*, a canonical marker for mononuclear phagocytes, was identified in nine clusters of our dataset. Four clusters were annotated as microglia (MG), one as macrophages (MF) and four as dendritic-like cells (DC-like) (**Figure 2B** and **Table 1**).

MG clusters (MG1, MG2, MG3, MG4) differentially expressed zebrafish microglial genes such as the lipoproteins *apoc1* and *apoeb* (Herbomel, Thisse, and Thisse 2001; Peri and Nusslein-Volhard 2008; Ferrero et al. 2018; Mazzolini et al. 2019), *ms4a17a.10* (Oosterhof et al. 2018) - a member of the membrane-spanning 4A gene family-, galectin 3 binding protein *lgals3bpb* (Rovira et al. 2022; Kuil et al. 2019), and hepatitis A virus cellular receptors *havcr1* and *havcr2* (Kuil et al. 2019; Oosterhof et al. 2018) (**Figure 4A,D**). Moreover, *csf1ra* and *csf1rb*, the zebrafish paralogs of CSF1R and well conserved regulators of microglia development and homeostasis (Oosterhof et al. 2018; Ferrero et al. 2021; Hason et al. 2022), were also identified as marker genes, although their level of expression differed between microglia clusters (**Figure 4D**, **Table 1**). Importantly, expression of canonical microglial genes were also found in the MG clusters such as *p2ry12*, *hexb*, *mertka* and members of the *c1q* genes, among others, supporting a conserved microglial phenotype (Butovsky et al. 2014; Jurga, Paleczna, and Kuter 2020; Butovsky and Weiner 2018; Gerrits et al. 2020) (**Figure 4-supplement 1**).

We also found a cluster of *mpeg1.1*-expressing cells that we annotated as *non-microglia macrophages* (MF). Similar to the microglia clusters (MG), this cluster differentially expressed macrophage-related genes such as *marco*, *mfap4*, *csf1ra* and components of the complement system (e.g. *c1qb*) (**Figure 4B,D**, **Table 1**). However, this cluster differed from the four microglia clusters because microglia markers were not found. This cluster also showed high expression of calcium binding proteins such as *s100a10b*, *anxa5b* and *icn*, as well as the coagulation factor XIII *f13a1b*, among others (**Figure 4B,D** and **Table 1**). In contrast to mammals, the distinction between microglia and other macrophages in the adult zebrafish brain (i.e. border-associated macrophages) is still unclear (Silva et al. 2021) and to date, no known marker or fluorescent reporter line is available to distinguish these two related cell types. Another possibility is that these *mpeg1.1*-expressing cells are blood-derived macrophages. In order to better characterize these two *mpeg1.1*-expressing clusters we performed a differential expression analysis between MF and MG (all four clusters together). As shown in **Figure 4E**, microglial genes such as *apoeb*, *apoc1*, *lgals3bpb*, *ccl34b.1*, *havcr1* and *csf1rb* were significantly down-regulated, whereas

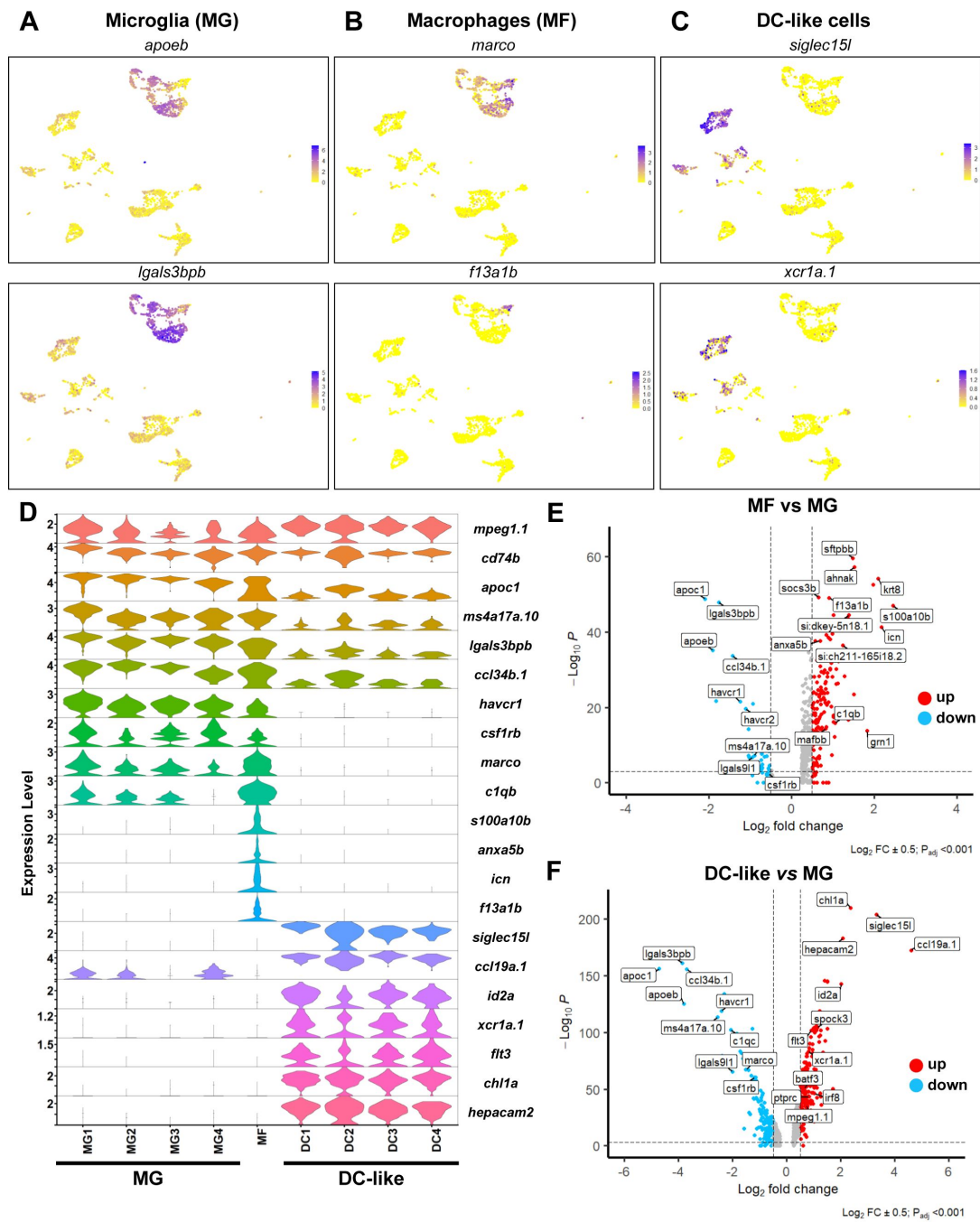


Figure 4.

Heterogenous subsets of mononuclear phagocytes exist in the zebrafish brain.

A-C. UMAP visualization of the expression of selected genes in the microglia (*apoeb* and *lgals3bbp*) (A), non-microglia macrophage (*marco* and *f13a1b*) (B) and DC-like (*xcr1a.1* and *siglec15l*) (C) cell clusters. Color scale (gradual from yellow to purple) indicates the expression level for each gene (normalized counts in log₁p). **D.** Violin plot analysis comparing the expression levels of selected genes (y-axis, normalized counts in log₁p) between the different mononuclear phagocyte cell clusters. **E.** Volcano plot showing the differentially expressed (DE) genes between microglia (MG) and non-microglia macrophages (MF). Lines indicate significantly DE genes (\log_2 fold-change > |0.5|, $-\log_{10} P_{adj} < 0.001$). Red dots represent up-regulated genes and blue dots down-regulated genes. Labels show representative DE genes identified in the analysis. **F.** Volcano plot showing the DE genes between microglia (MG) and DC-like cells (DC-like). Lines indicate significantly DE genes (\log_2 fold-change > |0.5|, $-\log_{10} P_{adj} < 0.001$).

macrophage-related genes such as *s100a10b*, *sftpbb*, *icn*, *fthl27*, *anxa5b*, *f13a1b* and *spi1b* were significantly up-regulated (**Table 3**). Therefore, these genes may thus serve as novel markers to discriminate these two related types of macrophages.

Finally, our analysis identified a third group of *mpeg1.1*-expressing cells represented in four clusters (DC1, DC2, DC3, DC4) and annotated as DC-like (**Figure 2B**). Highly expressed genes in these clusters included *siglec15l* (sialic acid binding Ig-like lectin 15, like) and *ccl19a.1* (C-C motif ligand 19a), a putative ligand of the zebrafish T cell receptor *ccr7* (Wu et al. 2012) (**Figure 4C,D** and **Table 1**). Intriguingly, these four clusters expressed *id2a*, *xcr1a.1*, *batf3* (*basic leucine zipper ATF-like 3 transcription factor*), and *flt3* (**Figure 4C,D** and **Table 1**), which are the orthologs of the mammalian *Id2a*, *Xcr1*, *Batf3* and *Flt3* genes, required for development and/or functions of conventional dendritic cells (cDC1) (Cabeza-Cabrerizo et al. 2021). These clusters also expressed *chl1a* (adhesion molecule L1), reported to promote DC migration through endothelial cells (Maddaluno et al. 2009) and *hepacam2* (**Figure 4D**, **Table 1**), frequently found in mammalian DC expression datasets. However, all four clusters had negligible expression of any of the microglia or macrophage markers previously mentioned (**Figure 4D**, **Table 1**). Based on their transcription profile and possible shared characteristics with mammalian DCs, these clusters were annotated as DC-like cells (DC1, DC2, DC3, DC4).

We next conducted a differential expression analysis of DC-like cells (DC1, DC2, DC3, DC4) versus MG (MG1, MG2, MG3, MG4), as two separate clusters. As shown in **Figure 4F**, significantly different genes include genes previously found as DC-like (up-regulated) or microglial (down-regulated) markers, thus confirming their distinct transcriptomic profiles. In addition DC-like cells could also be identified based on differential expression of *irf8*, *ptprc* and *mpeg1.1*, all significantly up-regulated in this population in comparison to MG (**Figure 4F**, **Table 3**). This is similar to mammalian cDC1, which are $IRF8^{\text{high}}$, $PTPRC(\text{CD}45)^{\text{high}}$ and $MPEG1^{\text{high}}$ (Cabeza-Cabrerizo et al. 2021), and thus strengthens the idea that DC-like cells phenotypically resemble mammalian cDC1. In order to explore the biological function of MG and DC-like cells, we performed pathway enrichment analysis (using GO Biological Processes and Reactome) for each MG and DC-like markers (**Table 4** and see **Materials and Methods**). This analysis enriched for terms in MG such as *endosomal lumen acidification* (e.g. H+ ATPase family genes), *synapse pruning* (e.g. *C1QC/c1qc*), *response to lipoprotein particle* (e.g. *ABCA1/abca1b*, *APOE/apoeb*), *interleukin-10 signalling* (e.g. *IL10RA/il10ra*), *macrophage activation* (e.g. *CTSC/ctsc*, *HAVCR2/havcr2*), *MHC class II antigen presentation* (e.g. *CD74/cd74a*, *HLA-DOB/mhc2b*), *complement cascade* (e.g. *C1QA/c1qa*, *CFP/cfp*), *mononuclear cell migration* (e.g. *CSF1R/csf1rb*, *CMKLR1/cmklr1*) or *phagocytosis* (e.g. *MERTK/merkta*, *MARCO/marco*) (**Figure 4 supplement 2A**, **Table 4** and see **Materials and Methods**). Enriched terms in DC-like included *FLT3 signaling* (e.g. *FLT3/flt3*), *myeloid cell differentiation* (e.g. *BATF3/batf3*, *ID2/id2a*), *Rac2 GTPase cycle* (e.g. *RAC2/rac2*, *CDC42/cdc42l*), *Fc receptor signaling pathway* (e.g. *FCER1G/fcer1g*), *cell chemotaxis* (e.g. *CCL19/ccl19a.1*, *XCR1/xcr1a.1*), innate signaling pathways such as *toll-like receptor cascades* (e.g. *TLR6/tr1*, *IRAK3/irak3*) as well as terms involved in adaptive immunity such as *alpha-beta T cell activation* (e.g. *CBLB/cblb*, *SOCS1/socs1*) or *lymphocyte activation involved in immune response* (e.g. *IL12B/il12ba*) (**Figure 4-supplement 2B**). Moreover, we used the Enrichr tool to predict the annotation of the MG and DC-like clusters using the PanglaoDB database that contains multiple single-cell RNA sequencing experiments from mouse and human (Franzen, Gan, and Bjorkegren 2019). The three top significant cell types for MG marker genes were “microglia”, “monocytes” and “macrophages” while for DC-like were “Dendritic Cells”, “Plasmacytoid DCs” and “Langerhans Cells” (**Figure 4-supplement 2C,D**).

DC-like cells as a parenchymal population along with microglia

Having demonstrated the diversity of the immune landscape of the adult zebrafish brain, we next sought to investigate the tissue localization of the different leukocyte populations identified in our data set, using the same transgenic lines as in **Figure 1**. To differentiate microglia from the two phenotypically distinct populations of brain mononuclear phagocytes (MF and DC-like), we first

examined adult brain sections of *Tg(mpeg1:GFP)* and *Tg(p2ry12::p2ry12-GFP)* single transgenic fish immunolabeled for GFP and the pan-leukocytic marker L-plastin (Lcp1). We found the majority of L-plastin⁺ cells within the brain parenchyma co-expressed the *mpeg1:GFP* transgene (**Figure 5A-C**). Upon examination of *Tg(p2ry12::p2ry12-GFP)* fish, however, we observed that not all parenchymal L-plastin⁺ cells were GFP (**Figure 5D-F**). Analysis of *Tg(p2ry12::p2ry12-GFP; mpeg1:mCherry)* double transgenics confirmed these observations, a.k.a that a fraction of *mpeg1:mCherry*⁺ cells was negative for the microglial *p2ry12::p2ry12-GFP* transgene (**Figure 5G-J**). Interestingly, in contrast to GFP⁺; mCherry⁺ microglia which are abundant across brain regions, GFP⁻ mCherry⁺ cells particularly localized in the ventral part of the posterior brain parenchyma (midbrain and hindbrain) (**Figure 5G-J**). Notably, these cells presented with a highly branched morphology when compared to GFP⁺; mCherry⁺ microglia.

Based on these findings, we next investigated brain samples from *Tg(mhc2dab:GFP; cd45:DsRed)* fish, where co-expression of both fluorescent reporters specifically labels mononuclear phagocytes (Wittamer et al. 2011; Ferrero et al. 2018). In our previous work, we had already observed that, in the brain of these animals, two phenotypically distinct cell populations could be isolated by flow cytometry based on differential *cd45:DsRed* expression levels. While the *cd45*^{low}; *mhc2*⁺ fraction was clearly identified as microglia due to their specific expression of *apoeb* and *p2ry12*, the exact identity of the *cd45*^{high}; *mhc2*⁺ cells remained unclear. However, we initially found these cells lack expression of *csf1ra* transcripts (Ferrero et al. 2018) which, in light of our single cell transcriptomic data, excluded them as macrophages and point to a DC-like cell identity. So, to evaluate the tissue localization of *cd45*^{high}; *mhc2*⁺ cells, we performed direct imaging of transgene fluorescence on vibratome brain sections from *Tg(mhc2dab:GFP; cd45:DsRed)* fish (**Figure 5K**). Most GFP⁺ cells were DsRed negative, suggesting the low expression of the *cd45* transgene in microglia likely precluded direct imaging of DsRed in these cells. However, in the ventral part of the posterior brain (midbrain and hindbrain), we observed a clear population of GFP⁺; DsRed⁺ cells, with a highly ramified morphology (**Figure 5L-N**). The reliable detection of endogenous DsRed signal in these cells likely identified them as DsRed^{high}. Altogether, these observations strongly pointed to *mpeg1*⁺; *p2ry12*⁻ and *cd45*^{high}; *mhc2*⁺ cells as being the same parenchymal non microglial population.

Finally, we also examined the localization of neutrophils and lymphoid cells, labeled using the *Tg(mpx:GFP)*, *Tg(lck:GFP)* and *Tg(ighm:GFP)* lines, respectively (**Figure 5-supplement 1**). In accordance with *mpeg1*⁺; *Lcp1*⁺ cells being the main leukocyte population present in the adult zebrafish brain parenchyma and with our previous flow cytometry analysis, *mpx*⁺, *lck*⁺ and *ighm*⁺ cells were rarely found and, if present, they were located at the border of the sections or lining the ventricles (**Figure 5-supplement 1**).

Collectively, our findings demonstrated that, in addition to microglia, the steady-state brain parenchyma of the adult zebrafish brain contains phenotypically distinct populations of mononuclear phagocytes with a restricted spatial localization within the tissue. Importantly, these two populations are easily distinguished using a combination of available transgenic lines.

Transcriptomic analysis of microglia and DC-like cells sorted using different reporter lines

To determine whether brain *mpeg1:mCherry*⁺; *p2ry12:GFP*⁻ and *cd45:DsRed*^{high}; *mhc2:GFP*⁺ cells do indeed represent a unique population of DC-like cells, we next performed bulk transcriptomic analyses to compare their expression profile. As a source for these studies, we used both *Tg(p2ry12::p2ry12-GFP; cd45:DsRed)* and *Tg(mhc2dab:GFP; cd45:DsRed)* adult fish, allowing to FACS-sort microglia identified in these animals as GFP⁺; DsRed⁺ or GFP⁺; DsRed^{low} cells, respectively (Ferrero et al. 2018). Brain putative DC-like cells were obtained using the *Tg(mhc2dab:GFP; cd45:DsRed)* reporter, and isolated as GFP⁺; DsRed^{high} (**Figure 6A-C**).

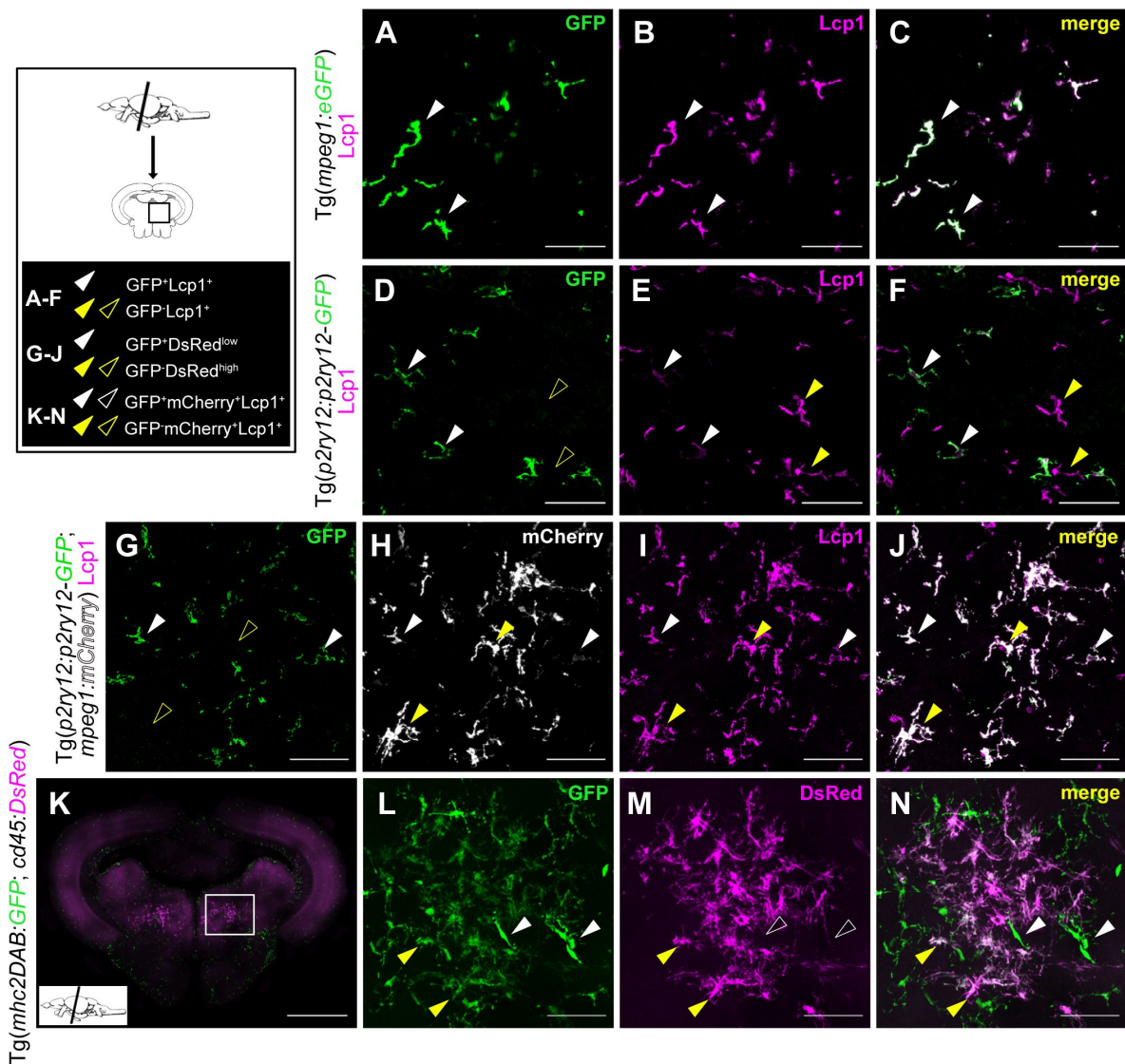


Figure 5.

DC-like cells localize together with microglia within the brain parenchyma.

A-F. Immunofluorescence on transversal brain sections (14 μm) from *Tg(mpeg1:GFP)* (A-C) or *Tg(p2ry12:p2ry12-GFP)* (D-F) transgenic adult fish co-immunostained with anti-GFP (green) and anti-Lcp1 (magenta) antibodies. **A-C.** All *mpeg1:GFP*⁺ mononuclear phagocytes in the brain parenchyma display Lcp1 immunostaining, as expected. **D-F.** Similarly, all microglial cells, identified by GFP expression in the brain parenchyma of *Tg(p2ry12:p2ry12-GFP)* fish, are Lcp1⁺, as expected. **G-J.** In sections of adult *Tg(p2ry12:p2ry12-GFP; mpeg1:mCherry)* double transgenic animals, GFP labeling is not observed in all mCherry⁺ cells. GFP (green), mCherry (grey), Lcp1 (magenta) and merge of the three channels. All images were taken using a 20X objective and correspond to orthogonal projections. White arrowheads point to microglial cells (GFP⁺; Lcp1⁺ or GFP⁺; mCherry⁺; Lcp1⁺) and yellow arrowheads to DC-like cells (GFP⁺; Lcp1⁺ or GFP⁺; mCherry⁺; Lcp1⁺). Scale bars: 50 μm . **L-O.** Confocal imaging of a midbrain vibratome section (100 μm) from an adult *Tg(mhc2dab:GFP; cd45:DsRed)* brain. GFP (green), DsRed (magenta) and merge of the two channels are shown. Images correspond to orthogonal projections, white arrowheads point to GFP⁺; DsRed⁺ cells and yellow arrowheads to GFP⁺; DsRed^{high}. Scale bar in (K): 100 μm , scale bar in (L-N): 50 μm .

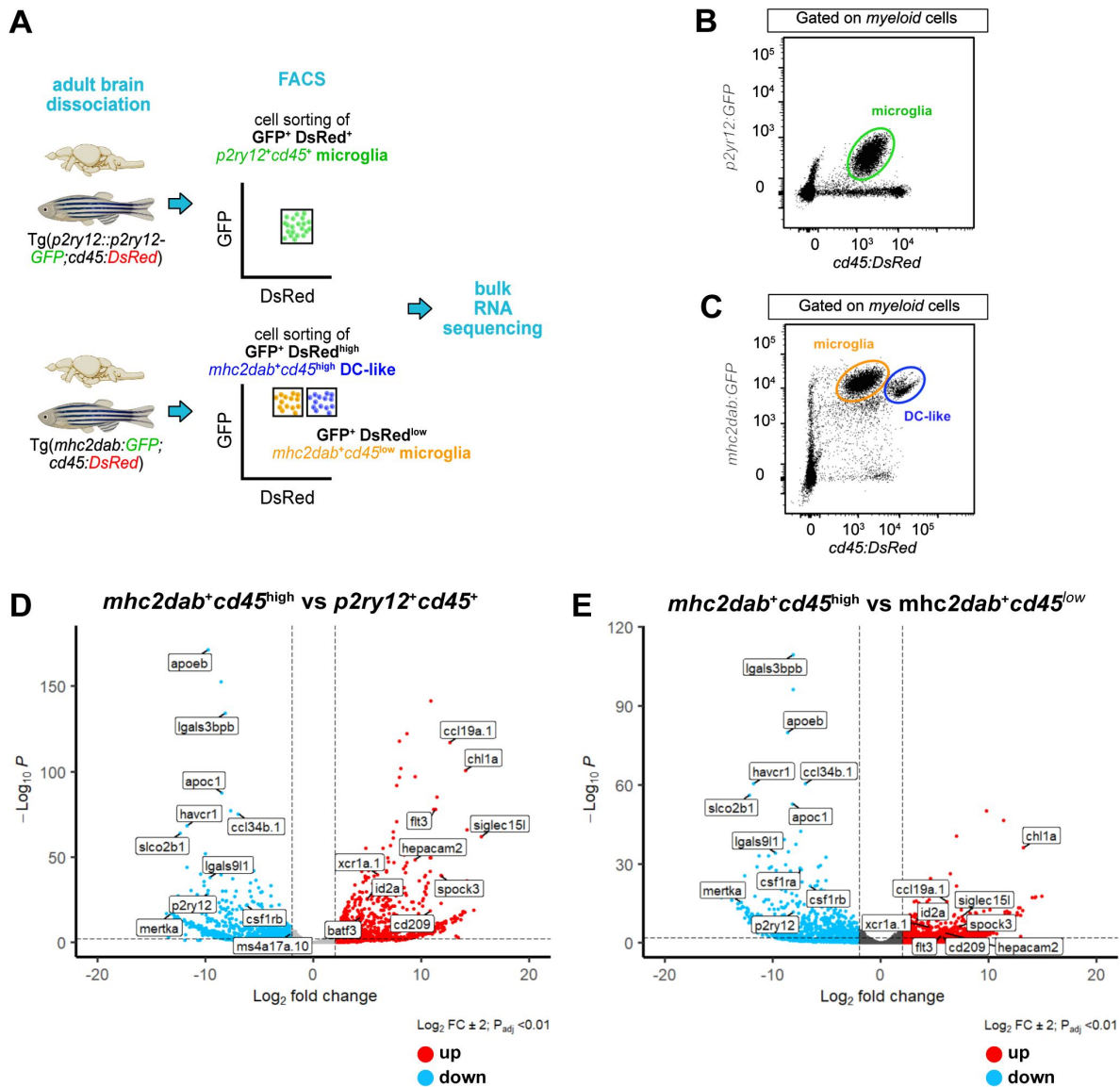


Figure 6.

Transcriptomic analysis of microglia (*p2ry12*⁺; *cd45*⁺ or *mhc2dab*⁺; *cd45*^{low}) and DC-like cells (*mhc2dab*⁺; *cd45*^{high}).

A. Schematic overview of the experiments. Microglia were isolated using *Tg(p2ry12::p2ry12-GFP; cd45:DsRed)* or *Tg(mhc2dab::GFP; cd45:DsRed)* transgenic fish, and DC-like cells using the *Tg(mhc2dab::GFP; cd45:DsRed)* reporter line. **B.** Representative flow cytometry plot identifying microglial cells in brain cell suspensions from *Tg(p2ry12::p2ry12-GFP; cd45:DsRed)* fish. **C.** Representative flow cytometry plot identifying *mhc2dab::GFP*⁺; *cd45:DsRed*^{low} microglia from *mhc2dab::GFP*⁺; *cd45:DsRed*^{high} DC-like cells in brain cell suspensions from *Tg(mhc2dab::GFP; cd45:DsRed)* fish. **D.** Volcano plot showing the differentially expressed (DE) genes between *mhc2dab*⁺; *cd45*^{high} DC-like cells and *p2ry12*⁺; *cd45*⁺ microglia. Red dots represent up-regulated genes and blue dots down-regulated genes. Lines indicate significantly DE genes (\log_2 fold-change $> |2|$, $-\log_{10} P_{adj} < 0.01$). Labels show marker genes for DC-like cells and microglia identified in the scRNA-sequencing analysis. **E.** Volcano plot showing the DE genes between *mhc2dab*⁺; *cd45*^{high} DC-like cells (blue) and *mhc2dab*⁺; *cd45*^{low} microglia (red). Lines indicate significantly DE genes (\log_2 fold-change $> |2|$, $-\log_{10} P_{adj} < 0.01$).

Differential expression analysis between *mhc2dab:GFP*⁺; *cd45:DsRed*^{high} – or putative DC-like cells – and *p2ry12:GFP*⁺; *cd45:DsRed*⁺ – or microglia – showed up-regulation of DC-like genes previously found in our single-cell transcriptomic analysis (**Figure 6D** [↗](#), **Table 5**). Similar results were obtained when comparing DC-like cells with microglia FACS-sorted as *mhc2dab*⁺; *cd45*⁺ cells (**Figure 6E** [↗](#), **Table 5**). These analyses confirm that our annotated DC-like cluster and *cd45:DsRed*^{high}; *mhc2dab:GFP*⁺ cells share a similar transcriptome distinct from microglia.

Interestingly, a recent study reported the presence of two heterogeneous populations of *mpeg1*-expressing cells in the adult zebrafish brain. These cells, which were annotated as *phagocytic* and *regulatory* microglia, and could be discriminated based on differential expression of the *ccl34b.1:GFP* reporter (Wu et al. 2020 [↗](#)). Interestingly, these two populations displayed a similar morphology, neuroanatomical location and differential gene expression pattern than the annotated DC-like and microglia populations identified in our dataset. We thus re-analyzed the data from Wu et al.. Differential expression between *regulatory* (*ccl34b.1*; *mpeg1*⁺) and *phagocytic* (*ccl34b.1*⁺; *mpeg1*⁺) cells demonstrated up-regulation of genes such as *siglec15l*, *spock3*, *chl1a*, *flt3*, *hepacam2*, *ccl19a.1*, *id2a* and *epdl1*, and down-regulation of genes such as *p2ry12*, *ccl34b.1*, *apoeb*, *apoc1*, *lgals3bpb*, *lgals9l1* and *havcr1*, among others (**Figure 6-supplement 1A and Table 5**). Notably, a large proportion of these DE genes overlapped with that previously found when comparing *mhc2dab:GFP*⁺; *cd45:DsRed*^{high} DC-like cells and *p2ry12:GFP*⁺; *cd45:DsRed*⁺ microglia (**Figure 6-supplement 1B,C and Table 5**). B cell-related genes such as *ighz* and *pax* were up-regulated (**Figure 6-supplement 1A**), suggesting the presence of B cells in the *ccl34b.1*; *mpeg1*⁺ fraction, as expected (Ferrero et al. 2020 [↗](#); Moyses and Richardson 2020 [↗](#)). In addition, the expression profile of *ccl34b.1*⁺; *mpeg1*⁺ *phagocytic* microglia strongly correlated with that of *p2ry12:GFP*⁺; *cd45:DsRed*⁺ and *mhc2dab:GFP*⁺; *cd45:DsRed*⁺ microglia (0.76 and 0.71, respectively), whereas *ccl34b.1*⁺; *mpeg1*⁺ *regulatory* microglia correlated with *mhc2dab:GFP*⁺; *cd45:DsRed*^{high} DC-like cells (0.57) (**Figure 6-supplement 1D,E and Table 5**). Collectively, these findings suggest that, at the transcriptomic level, *ccl34b.1*⁺; *mpeg1.1*⁺ cells correspond to microglia in our dataset, and *ccl34b.1*⁺; *mpeg1*⁺ cells resemble the population we annotated as DC-like cells.

DC-like cells are located in the brain parenchyma and are *batf3*-dependent

Our results so far suggested the existence of a putative DC-like cell population located in the parenchyma of the healthy zebrafish brain. To strengthen our findings, we next developed a strategy to assess the identity of this population. We reasoned that the development of the zebrafish counterparts of mammalian cDC1 would likely rely on a conserved genetic program. In our single-cell transcriptomic analysis, zebrafish DC-like cells expressed *batf3*, a cDC1-required transcription factor in human and mouse (Cabeza-Cabrero et al. 2021 [↗](#)). Therefore, using CRISPR/Cas9 technology we generated a zebrafish *batf3* mutant as a model to explore the lineage identity of putative zebrafish DC-like cells. This mutant line carries a 8-bp deletion downstream of the ATG start, leading to a frameshift mutation and the generation of three premature stop codons (**Appendix 2-Figure 7**). The resulting protein lacks the DNA binding and basic-leucine zipper domains and is likely to be non-functional. To evaluate whether brain DC-like cells were present in these animals, we crossed the *batf3* mutant line to *Tg(p2ry12:p2ry12-GFP; mpeg1:mCherry)* double transgenic fish, and performed immunostainings of adult brain sections (**Figure 7A-J** [↗](#)). Because DC-like cells are abundant in the ventral posterior brain, we quantified the dorsal (mostly containing the optic tectum) and ventral areas separately, as well as the whole section. The numbers of *GFP*⁺; *mCherry*⁺; *Lcp1*⁺ microglia were similar to their *wild-type* siblings, whereas the ventral posterior brain of homozygous *batf3* mutants was largely devoid of *GFP*⁺; *mCherry*⁺; *Lcp1*⁺ cells, which identify DC-like cells in our model (**Figure 7K-M** [↗](#)). Moreover, we did not observe any changes in the density of other brain leukocytes (**Figure 7-supplement 1A-C**). Flow cytometry analyses of brain cell suspensions confirmed the dramatic loss of *GFP*⁺; *mCherry*⁺ cells in the absence of *batf3* ($2.98\% \pm 0.588$, $n=6$ versus 0.77 ± 0.097 , $n=10$) (**Figure 7 N,O** [↗](#)). Notably, expression of DC-like markers was barely detectable in the remaining *GFP*⁺; *mCherry*⁺ cells

(**Figure 7-supplement 1D,E**). However, these cells also displayed lower mCherry signal intensity, suggesting they most likely represent *mpeg1*-expressing MF or B cells (**Figure 7-supplement 1F,G**). Regarding GFP⁺; mCherry⁺ microglia, their proportion was unchanged when compared to that of control fish (**Figure 7 N,O**), which is concordant with our initial observations. Finally, we also performed direct imaging of transgene fluorescence on vibratome brain sections of *batf3* mutants carrying the *cd45:DsRed* transgene. In line with our observations, we found that loss-of-function of *batf3* in *Tg(cd45:DsRed)* transgenic fish resulted in the complete absence of DsRed^{high} DC-like cells in the ventral area of the midbrain parenchyma in comparison with control brains (**Figure 7-supplement 1H-K**). Collectively, these results demonstrated that, the population we annotated as DC-like cells is *batf3*-dependent similar to mammalian cDC1. These results reinforced our hypothesis that these cells represent the zebrafish counterparts of mammalian cDC1.

Characterization of microglia and dendritic-like cells in mononuclear phagocyte-deficient mutants

The presence of two distinct mononuclear phagocyte subsets in the brain parenchyma made us wonder about their respective status in commonly used microglia-deficient zebrafish lines, as they were all initially characterized using the pan-mononuclear phagocyte *Tg(mpeg1:GFP)* reporter (Oosterhof et al. 2018; Ferrero et al. 2021; Wu et al. 2020). With the ability to discriminate between both populations of microglia and DC-like cells, we thus next sought to examine in more details the phenotype of the *irf8*^{-/-}, *csf1ra*^{-/-}, *csf1rb*^{-/-} and *csf1ra*^{-/-}; *csf1rb*^{-/-} double mutant (*csf1r*^{DM}) alleles. To do so, we crossed each mutant line to *Tg(p2ry12:p2ry12-GFP)* animals and analyzed brain sections costained for GFP and L-plastin (**Figure 8**). According to our model, in this setup microglia will be labeled as GFP⁺; Lcp1⁺, while GFP⁻; Lcp1⁺ cells will mostly include DC-like cells, easily identified based on their typical ramified cell shape (**Figure 8A-D**). In addition to DC-like cells, GFP⁻; Lcp1⁺ cells may also include lymphocytes and/or neutrophils, which are anyway in much lower numbers than mononuclear phagocytes in the adult brain (**Figure 1D**).

IRF8 is a transcription factor essential for the development of mononuclear phagocytes in vertebrates (Yanez and Goodridge 2016), including zebrafish (Ferrero et al. 2020), where absence of *irf8* results in lack of microglia (Shiau et al. 2015; Earley, Graves, and Shiau 2018). In line with these findings, we found that adult *irf8* homozygous displayed a dramatic, albeit not complete, reduction of GFP⁺ microglial cells (**Figure 8E-H, U,W**). Interestingly, most remaining microglia localized near or along the ventricle borders, and exhibited characteristics reminiscent of an immature phenotype, e.g. a circular shape with few and short cellular processes (**Figure 8-supplement 1**). In this mutant, the density of GFP⁻; Lcp1⁺ DC-like cells was reduced in comparison to *wild-type* controls, in the ventral area (~50%) (**Figure 8U,W**).

As well-established regulators of zebrafish microglia, *csf1ra* or *csf1rb* deficiency had a strong effect on GFP⁺; Lcp1⁺ cells, with densities decreased ~50% in the dorsal and ventral areas. Interestingly, the density of GFP⁻; Lcp1⁺ DC-like cells was reduced in the ventral part of *csf1rb* homozygous fish (~50%), while it was doubled in *csf1ra*^{-/-} mutant animals in comparison to *wild-type* siblings (**Figure 8I-P, U,W**). Finally, we also examined fish lacking both *csf1r* paralogs (*Csf1r*^{DM}). These fish displayed a more severe phenotype, being devoid of both populations of microglia and DC-like cells, as indicated by the absence of GFP and Lcp1 signal (**Figure 8Q-W**). This is consistent with previous reports that *mpeg1:GFP*⁺ cells are depleted in the brain of *csf1r*^{DM} fish (Ferrero et al. 2021; Oosterhof et al. 2018).

Collectively, these results demonstrate the different mononuclear phagocyte-deficient zebrafish mutant lines have reduced numbers of microglia and exhibit distinct DC-like cell phenotypes. Our data also reveal that DC-like cells develop in an *irf8*-dependant manner, and identify possible opposite functions for the *csf1r* paralogs in the maintenance of this population.

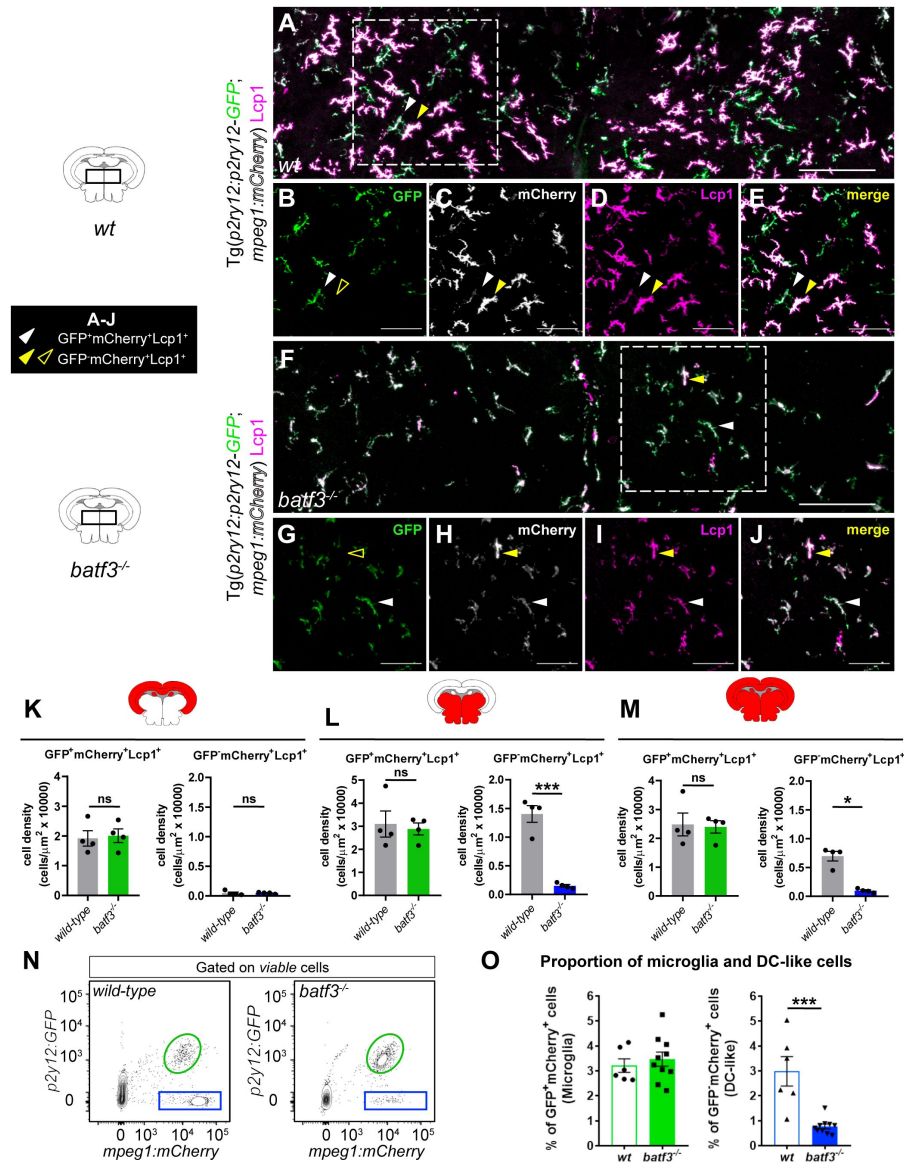


Figure 7.

Brain DC-like cells are lost in *batf3*^{-/-} mutant fish.

A-J. Immunofluorescence on transverse brain sections (14 μm) from adult *wild-type* (A-E) and *batf3*^{-/-} mutant (F-J) fish carrying the *Tg(p2ry12:p2ry12-GFP; mpeg1:mCherry)* double transgene and immunostained for GFP (green), mCherry (grey) and Lcp1 (magenta). Illustrative case of the merge of the three channels (A, F) allowing to identify GFP⁺; mCherry⁺; Lcp1⁺ microglia (white arrowheads) versus GFP⁺; mCherry⁺; Lcp1⁻ DC-like cells (yellow arrowheads). While DC-like cells are found in high numbers within the ventral part of control parenchyma (A), these are dramatically decreased following genetic loss of *batf3* (F). Scale bars: 100 μm. (B-E, G-J). Single channels high magnification of the insets in A (B-E) and F (G-J). Scale bars: 50 μm. Images were taken using a 20X objective and correspond to orthogonal projections. **K-M.** Quantification of cell density for GFP⁺; mCherry⁺; Lcp1⁺ microglia and GFP⁺; mCherry⁺; Lcp1⁻ DC-like cells in the dorsal midbrain area or optic tectum (K), ventral midbrain area (L) and the entire section (M) of control (grey bars) and *batf3*^{-/-} (green bars) fish. Each dot represents a single fish and data are mean ± SEM. * P < 0.05 (Mann-Whitney test), *** P < 0.0001 (Two-tailed unpaired t-test). **N.** Flow cytometry analysis of brain cell suspensions from *wild-type* and *batf3*^{-/-} adult fish carrying the *Tg(p2ry12:p2ry12-GFP; mpeg1:mCherry)* reporter. The GFP⁺; mCherry⁺ fraction identifies microglia (green circle), whereas the GFP⁺; mCherry⁻ fraction contains mainly DC-like cells (blue frame). **O.** Percentage of microglia and DC-like cells in brain cell suspensions for each genotype, relative to the whole living brain population, as shown in (N) (*wild-type*, n=6; *batf3*^{-/-}, n=10). *** P < 0.001 (Two-tailed unpaired t-test). n refers to number of biological replicates.

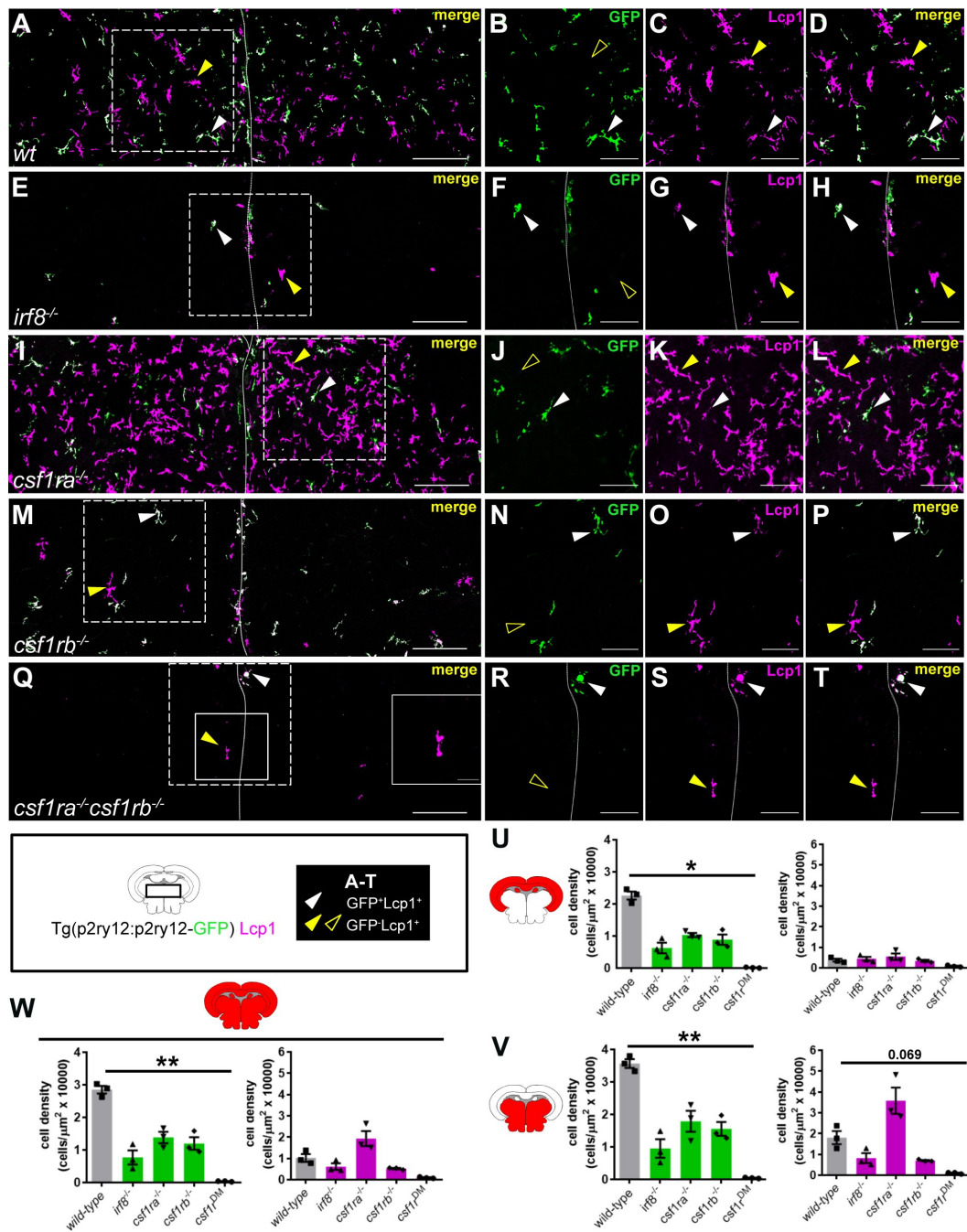


Figure 8.

Examination of microglia and DC-like cells in myeloid-deficient mutant lines.

A-D. Immunofluorescence on transverse brain sections from *Tg(p2ry12:p2ry12-GFP)* transgenic adult *wild-type* (A-D), *irf8^{-/-}* (E-H), *csf1ra^{-/-}* (I-L), *csf1rb^{-/-}* (M-P) and *csf1ra^{-/-}; csf1rb^{-/-}* (*csf1r^{DM}*) (Q-T) fish, co-stained with anti-GFP (green) and Lcp1 (magenta) antibodies. **A, E, I, M, Q.** For each genotype, illustrative case of the merge of the two channels, allowing to discriminate in the parenchyma GFP⁺; Lcp1⁺ microglia (white arrowheads) from GFP⁻; Lcp1⁺ DC-like cells (yellow arrowheads). Single channels high magnification of the insets (dashed frame) in A (B-D), E (F-H), I (J-L), M (N-P) and Q (R-T). Outline yellow arrowheads indicate the absence of GFP signal in corresponding yellow arrowhead pointed cells. Scale bar in (A), (E), (I), (M) and (Q) represents 100 μm and scale bar in other images 50 μm . **U-V.** Quantification of the cell density for GFP⁺ Lcp1⁺ microglia and GFP⁻ Lcp1⁺ DC-like cells in the dorsal (U), ventral (V) and whole area (W) of the brain for each genotype ($n=3$). Data in U-W are mean \pm SEM. * $P < 0.05$, ** $P < 0.01$ (Klusal-Wallis test with Dunn's post-hoc).

Discussion

In the present study, we have characterized the immune microenvironment of the adult zebrafish brain by profiling total $cd45^+$ leukocytes, isolated from transgenic reporter fish by FACS. First we show that, like in mammals, microglia constitute the predominant parenchymal immune cell in the brain of the adult zebrafish. Zebrafish microglia are identified based on several common canonical markers, some of which are previously reported to be conserved in mammals (Mazzolini et al. 2019 [↗](#); Silva et al. 2021 [↗](#); Oosterhof et al. 2018 [↗](#)). These include *apoeb*, *apoc1*, *lgals3bpb*, *ccl34b.1* and *p2ry12*. Notably, we used different combinations of fluorescent reporter lines for the prospective isolation of adult microglia and found these genes to be consistently expressed. In addition, our observations also support a phenotypical heterogeneity of adult zebrafish microglia in the steady state by identifying several clusters sharing this microglia core signature, with different expression levels. This is in line with recent advances in our understanding of microglia diversity in human and mouse, and which revealed the presence of molecularly distinct microglia subtypes across developmental stages, specific brain regions or disease conditions (Stratoulias et al. 2019 [↗](#); Masuda et al. 2020 [↗](#)).

Although the notion of microglia heterogeneity in zebrafish is already proposed (Silva et al. 2021 [↗](#); Wu et al. 2020 [↗](#)), a major finding of our study is that, surprisingly, not all parenchymal mononuclear phagocytes qualify as microglial cells. Here we provide evidence that a proportion of myeloid cells in the healthy brain parenchyma is phenotypically distinct from microglia and identify as the zebrafish counterpart of mammalian cDC1. These cells, despite sharing the microglial expression of *mpeg1.1* and genes involved in antigen presentation, display a unique transcriptomic profile characterized by a core gene signature resembling that of mammalian cDC1 ($flt3^+$, $irf8^{high}$, $batf3^+$, $id2^+$, $xcr1^+$) but lacking canonical microglia markers. The lineage identity of these cells (referred to as DC-like cells), is further supported by their dependency to *batf3*, a key transcription factor for cDC1 development in mammals. In contrast, zebrafish microglia develop normally in absence of *batf3*, which highlights the reliance of both populations on distinct developmental programs. This notion is also reinforced by demonstrating that, unlike microglia, zebrafish brain DC-like cells are *csf1ra*-independent. However, both populations are controlled by *irf8*, a well-established regulator of microglia differentiation and DC development in mammals (Van Hove et al. 2019 [↗](#); Cabeza-Cabrerizo et al. 2021 [↗](#)).

Previously, two independent studies have reported the existence of an immune cell population with a similar expression profile to DC-like cells in the juvenile and adult zebrafish brain (Wu et al. 2020 [↗](#); Silva et al. 2021 [↗](#)). However, contradictory conclusions were drawn regarding the identity of these cells. In one study using bulk RNAseq, a cell population expressing *id2a*, *ccl19a.1*, *siglec15l*, but not *apoeb* or *lgals3bpb*, was identified and categorized as a phenotypically distinct microglia subtype (Wu et al. 2020 [↗](#)). This population could be discriminated from other *mpeg1*-expressing parenchymal cells notably by the lack of Tg(*ccl34b.1:GFP*) transgene expression. Interestingly, while $ccl34b.1^+$; $mpeg1^+$ microglia were widely spread across brain regions, $ccl34b.1^+$ $mpeg1^+$ cells showed a restricted spatial localization in the white matter. In addition, these cells also displayed a highly ramified morphology as well as independency of *csf1ra* signaling, all reminiscing the DC-like cells identified in our study. However, in another report using single-cell RNAseq, a comparable myeloid population expressing high levels of *mpeg1* as well as *ccl19a.1*, *flt3*, *siglec15l*, among other DC-like genes, was labeled as brain macrophages, owing to the absence of microglial-specific markers such as *p2ry12*, *csf1ra*, *hexb* and *slc7a7* (Silva et al. 2021 [↗](#)). The present work resolves these apparent contradictions, and provides new insights into the identity of this cell population. We report here that $ccl34b.1^+$; $mpeg1^+$ cells display a similar gene signature to the DC-like cells identified in our analyses. This strongly suggests that the $ccl34b.1^+$; $mpeg1^+$ and $p2ry12^+$; $mpeg1^+$ populations share a similar cellular identity. Likewise, the anatomical location of the brain macrophage cluster identified by Silva and colleagues was not investigated, but based on their dominated expression profile by key DC markers, these cells likely represent the equivalent of the $p2ry12^+$; $mpeg1^+$ cell population. Thus, based on the evidence that these three populations

constitute a unique cell type, and coupled to the demonstration that *in vivo* *p2ry12*⁻; *mpeg1*⁺ cells are reliant on *batf3*, collectively these features imply these cells share more similarities with mammalian DCs than with microglia or macrophages. Therefore, with respect to their morphology, transcriptomic profile and *batf3*-dependency, we propose this population as DC-like cells rather than microglia and/or macrophages.

One important question raised from these new findings could relate to the abundance of DC-like cells within the healthy zebrafish brain parenchyma, which is strongly different than what is known in mammals. Indeed, while murine DCs are naturally found at the brain border regions such as the meningeal layers and the choroid plexus – structures in contact with the brain microenvironment- (Van Hove et al. 2019 [↗](#)) their presence within the healthy brain parenchyma is scarce and somewhat controversial. In mammals, infiltration of functional DCs in the brain parenchyma occurs with age (Kaunzner et al. 2012 [↗](#)), or following an injury or infection, where they act as important inducers of the immune response through activation of primary T cells and cytokine production (Ludewig et al. 2016 [↗](#)). In addition, DC infiltration is a hallmark of several neurological diseases and aging, and is believed to contribute to the establishment of a chronic neuroinflammatory state (Ludewig et al. 2016 [↗](#)). In this regard, Wu et al. previously reported that *ccl34b.1* *mpeg1*⁺ cells - or DC-like cells - exhibit functional differences, including limited mobility and phagocytic properties, and enhanced release of immune regulators following bacterial infection, when compared to *ccl34b.1*⁺ *mpeg1*⁺ microglia. The same study also proposed that zebrafish *ccl34b.1*; *mpeg1*⁺ cells might play a regulatory role by recruiting T lymphocytes in the brain parenchyma upon infection (Wu et al. 2020 [↗](#)). These biological features suggest that brain DC-like cells might exhibit APC functions. However, due to a lack of tools this hypothesis is currently difficult to address. There is evidence that DC functionalities are conserved in teleosts (Lugo-Villarino et al. 2010 [↗](#); Bassity and Clark 2012 [↗](#)), but the process of antigen presentation in zebrafish remains poorly understood (Lewis, Del Cid, and Traver 2014 [↗](#)). Because zebrafish lack apparent lymph nodes and the secondary lymphoid structures found in mammals, it is not known where stimulation of naive T cells takes place and whether fish have developed unique ways to mount an adaptive immune response. Therefore, although a comprehensive analysis of the anatomical zone enriched in DC-like cells requires further investigation, from an evolutionary perspective, it is tempting to speculate that the specific localization of zebrafish DC-like cells in the ventral brain tissue might provide an environment to facilitate antigen detection and/or presentation in this organ. Future work using the mutants as described in this study in addition to new DC-like-specific reporter lines will help addressing such exciting questions.

Furthermore, our work sheds light on the myeloid brain phenotype of mutant lines commonly used by the fish macrophage/microglia community. CSF1R is a master regulator of macrophage development and function in vertebrates which is found in two copies (*csf1ra* and *csf1rb*) in zebrafish due to an extra genome duplication. Others and we have contributed to the uncovering of the relative contribution of each paralog to the ontogeny of zebrafish mononuclear phagocytes (Herbomel, Thisse, and Thisse 2001 [↗](#); Ferrero et al. 2021 [↗](#); Hason et al. 2022 [↗](#); Oosterhof et al. 2018 [↗](#)). Here we also provide a new level of precision regarding these processes. As reported, the density of all parenchymal *mpeg1:GFP*⁺ mononuclear phagocytes is reduced in the brain of single *csf1ra*^{-/-} and *csf1rb*^{-/-} adult mutant fish, and these cells completely disappear when both genes are knocked out (Oosterhof et al. 2018 [↗](#); Ferrero et al. 2021 [↗](#)). Using *in vivo* lineage tracing, we previously demonstrated that zebrafish microglia are established in two successive steps, with a definitive wave of hematopoietic stem cell (HSC)-derived adult microglia replacing an embryonic/primitive population. In addition, we showed that in *csf1rb*^{-/-} fish remaining *mpeg1:GFP*⁺ cells are of primitive origin, whereas in *csf1ra*^{-/-} fish they are of definitive origin (Ferrero et al. 2021 [↗](#)). Collectively, these observations have led to a model in which embryonic-derived microglia make up the majority of remaining *mpeg1*-expressing cells in *csf1rb*^{-/-} fish, while residual cells represent adult microglia in the *csf1ra*^{-/-} line, but at a strongly reduced cell number relative to controls. However, adult microglia in these experiments were identified based on the concomitant *mpeg1:GFP* transgene expression and the HSC lineage tracing marker, a strategy that,

retrospectively, did not allow to discriminate them from the DC-like cells described in this study. Here, we sought to test these models in light of our current findings, and especially following the observation that individual mutant fish exhibit opposite brain DC-like phenotypes, with DC-like cell numbers being strongly increased or decreased in *csf1ra*^{-/-} and *csf1rb*^{-/-} animals, respectively. In mammals, DCs are produced by HSCs in the bone marrow so the reduced numbers of DC-like cells in *csf1rb*^{-/-} fish likely results from the defective HSC-derived definitive myelopoiesis that characterized this mutant (Ferrero et al. 2021 [↗](#); Hason et al. 2022 [↗](#)). Accordingly, the *csf1rb*^{-/-} line is devoid of both populations of adult microglia and DC-like cells and, as initially proposed, the most residual cells within the brain parenchyma represent remnants of embryonic microglia (Ferrero et al. 2021 [↗](#)). Conversely, the increased density of DC-like cells in *csf1ra*^{-/-} adult fish indicates that this paralogue is dispensable for the ontogeny of DC-like cells, but points to a possible role in controlling the DC-like cell growth and/or survival. This is in contrast with microglia, which we now found to be unambiguously depleted following a *csf1ra* loss-of-function. Therefore, these findings warrant an adjustment of the initial model, as the majority of remaining *mpeg1*-expressing cells in the *csf1ra*^{-/-} line correspond to DC-like cells, and not adult microglia. Notably, these results are consistent with the reported loss of *ccl34b.1*⁺; *mpeg1*⁺ cells in *csf1ra*^{-/-} fish by Wu and colleagues (Wu et al. 2020 [↗](#)), and with the observed upregulation of DC-like genes coupled to a downregulation of microglia markers in *mpeg1*:GFP cells isolated from the brain of *csf1ra*^{-/-} *csf1rb*^{+/-} mutant animals (Oosterhof et al. 2018 [↗](#)).

In zebrafish little is known regarding lymphoid cells in the adult CNS. Similar to DCs, lymphocytes are present in limited numbers in the healthy mammalian brain and mainly restricted to the meningeal layers, choroid plexus or the perivascular space (Mundt et al. 2019 [↗](#); Croese, Castellani, and Schwartz 2021 [↗](#)). In our transcriptomic analysis, we identified a heterogeneous repertoire of lymphoid cells: T, NK and ILCs. B lymphocytes, which could not be captured using the *cd45:DsRed* transgene (Wittamer et al. 2011 [↗](#)), were also detected using the *IgM*:GFP line, albeit in very low numbers. Our data suggest that, similar to mammals, in zebrafish lymphoid cells in the steady-state are only occasionally found in the brain parenchyma, and are most likely localized in the brain border regions. Here, it is worth noting that our protocol for brain dissection requires the removal of the skull, which may completely or partially disrupt the thin meningeal layers. Consequently, whether non parenchymal cells identified in this study are located in the meninges, in the choroid plexus or even in the blood circulation remains to be determined.

Although the innate counterparts of the lymphoid system (NK cells and ILCs) have been identified in different zebrafish organs (Hernández 2018; Silva et al. 2021 [↗](#); Tang et al. 2017 [↗](#)), the lack of specific fluorescent reporter lines has until now precluded a detailed characterization of these cell populations. In particular, as a recently discovered cell type in zebrafish (Hernández 2018), the phenotypic and functional heterogeneity of ILC-like cells are still poorly understood. In this study, we found that the adult zebrafish brain contains a population that resembles the ILC2 subset in mammals. Like human and mouse ILC2s, these cells do not express the T cell receptor *cd4-1*. However, these cells are positive for T_H2 cytokines *il13* and *il4*, and also express *gata3*, a transcription factor involved in ILC2 differentiation. Surprisingly, *lck* expression in our dataset was restricted to T lymphocytes and NK cells, whereas as in humans this gene is also expressed in all ILCs (Bjorklund et al. 2016 [↗](#)). A previous study in zebrafish reported populations representing all three ILC subtypes isolated from the intestine based on expression of the *lck*:GFP transgene (Hernández 2018). That suggests a conserved *lck* expression pattern across species. However, in none of these experiments the presence of ILCs in the *lck*:GFP negative fraction was investigated, so whether the absence of *lck* transcripts in our ILC2 dataset is due to a low detection sensitivity or a lack of expression remains an open question. Nevertheless, as we showed, the level of expression of ILC2 transcripts remain specifically unchanged in brain leukocytes in the context of T cell deficiency. This validates that ILC2 are indeed present in this organ. In line with this, innate-lymphoid-like cells differentially expressing *il4*, *il13* and *gata3* have been recently annotated in the juvenile zebrafish brain (Silva et al. 2021 [↗](#)).

To conclude, our study provides a single-cell transcriptomic dataset of different brain leukocyte populations, and may serve as a reference to better characterize the immune cell complexity of the zebrafish brain in the steady state. Similar to mammalian microglia, zebrafish microglia are identified based on several common canonical markers, some of which are conserved between species, but their diversity is still poorly understood. Therefore, future investigations will benefit from mapping microglia heterogeneity across the zebrafish brain as a complementary approach to single-cell transcriptomics for studying microglia functions in health and disease. Further work will also be needed to elucidate the functions of some of the cell types identified in this study, especially DC-like cells, and to elucidate whether this population maintains locally or is continually replenished by cells from the periphery.

Materials and methods

Zebrafish husbandry

Zebrafish were maintained under standard conditions, according to FELASA (Alestrom et al. 2019) and institutional (Université Libre de Bruxelles, Brussels, Belgium; ULB) guidelines and regulations. All experimental procedures were approved by the ULB ethical committee for animal welfare (CEBEA) from the ULB. The following lines were used: *Tg(mhc2dab:GFP_{LT})^{sd67}* (Wittamer et al. 2011), *Tg(ptprc:DsRed^{express})^{sd3}* (here referred to as *cd45:DsRed*) (Wittamer et al. 2011), *Tg(mpeg1.1:eGFP)^{gl22}* (here referred to as *mpeg1:GFP*) (Ellett et al. 2010), *Tg(mpeg1.1:mCherry)^{gl23}* (here referred to as *mpeg1:mCherry*) (Ellett et al. 2010), *TgBAC(p2ry12:p2ry12-GFP)^{hdb3}* (Sieger et al. 2012), *Tg(lck:lck-eGFP)^{cz1}* (here referred to as *lck:GFP*) (Langenau et al. 2004), *TgBAC(cd4-1:mcherry)^{UMC13}* (here referred to as *cd4-1:mCherry*) (Dee et al. 2016), *Tg(Cau.Ighv-ighm:EGFP)^{sd19}* (here referred to as *ighm:GFP*) (Page et al. 2013), *Tg(mpx:GFP)ⁱ¹¹³* (Mathias, Walters, and Huttenlocher 2009). The mutant lines used were: *panther^{4e1}* (here called *csf1ra^{-/-}*) (Parichy DM 2000); *csf1rb^{sa1503}*, generated via ethylnitrosurea (ENU) mutagenesis, were obtained from the Sanger Institute Zebrafish Mutation Project and previously characterized (Ferrero et al. 2021), *irf8^{std96}* (Shiau et al. 2015), *rag2^{E450fs}* (Tang et al. 2014). Special care was taken to control reporter gene dosage through experiments (with all control and mutant animals used in this study known to carry similar hemizygous or homozygous doses of the GFP transgenes). The term “adult” fish refers to animals aged between 4 months and 8 months old. For clarity, throughout the text, transgenic animals are referred to without allele designations.

Generation of *batf3^{-/-}* mutant zebrafish

The *batf3* (ENSDARG0000042577) knockout mutant line was generated using the CRISPR/Cas9 system. A single guide RNA (sgRNA) targeting the ATG start in the first exon (targeting sequence: GAAGTGATGCTCCAGCTCTA) was identified and selected for its highest on-target activity and lowest predicted off-target score using a combination of the Sequence Scan for CRISPR software (available at <http://crispr.dfci.harvard.edu/SSC/>) (Xu et al. 2015) and the CRISPR Scan (available at <http://www.crisprscan.org/>). The DNA template for the sgRNA synthesis was produced using the PCR-based short-oligo method as described (Talbot and Amacher 2014). The following primers were used: Fw: 5'-GCGATTTAGGTGACACTATA-3' and Rv: 5'-AAAGCACCAGCTCGTGCCAC-3'. The resulting PCR product was purified by phenol-chloroform extraction and used for *in vitro* transcription using SP6 RNA-polymerase (NEB, M0207). The resulting sgRNA was purified using the High Pure PCR Cleanup Microkit (Roche, 498395500). 60 pg sgRNA and 100 pg Cas9 protein (PNA Bio) were co-injected into one-cell stage *wild-type* embryos. The genotyping of both embryos and adults was performed using the following primers: *batf3* fw: 5'-ACTTGACAGTTTAAGCATGCCT-3' and *batf3* rv: 5'-GAACATACCTCGCTCTGTCG-3'. PCR amplicons were analyzed using a heteroduplex mobility assay (on a 8% polyacrylamide gel) to assess the presence of CRISPR/Cas9-induced mutations.

The *batf3^{ulb31}* line carries an 8-bp deletion in exon 1. The deletion introduces a frameshift after amino acid 16 of the predicted 121-amino acid ORF, followed by 8 heterologous amino acids and then three successive premature stop codons. Heterozygous F1 fish were backcrossed at least four generations with AB* *wild-types* before being crossed to *Tg(mhc2dab:GFP; cd45:DsRed)* fish, as well as *Tg(p2ry12:p2ry12-GFP; mpeg1:mCherry)* animals for phenotype assessment.

Flow cytometry and cell sorting

Cell suspensions from adult brains were obtained as previously described (Wittamer et al. 2011 [↗](#); Ferrero et al. 2021 [↗](#); Ferrero et al. 2018 [↗](#)). Briefly, adult brains dissected in 0.9X Dulbecco's Phosphate Buffered Saline (DPBS) were triturated and treated with Liberase TM at 33°C for 30-45 minutes, fully dissociated using a syringe with a 26G needle and washed in 2% fetal bovine serum diluted in 0.9X DPBS. Cell suspensions were centrifuged at 290g 4°C 10 min and filtered through a 40µm nylon mesh. Just before flow cytometry analysis, SYTOXTMRed (Invitrogen) was added to the samples at a final concentration of 5nM to exclude non viable cells. Flow cytometry acquisition and cell sorting was performed on a FACS ARIA II (Becton Dickinson). To perform the qPCR experiments, between 7,000-10,000 *cd45:DsRed*⁺ leukocytes and approximately 2,500 *p2ry12:GFP*⁺; *mpeg1:mCherry*⁺ microglia or *p2ry12:GFP*⁺; *mpeg1:mCherry*⁺ DC-like cells were sorted, collected in RLT Plus buffer (Qiagen) and flash frozen in liquid nitrogen. Analyses were performed using FlowJo software. For morphological evaluation, 100,000 *cd45:DsRed*⁺ sorted cells were concentrated by cytocentrifugation at 300g for 10 minutes onto glass slides using a Cellspin (Tharmac). Slides were air-dried, fixed with methanol for 5 minutes and stained with May-Grünwald solution (Sigma) for 10 minutes. Then, slides were stained with a 1:5 dilution of Giemsa solution (Sigma) in distilled water (dH₂O) for 20 minutes, rinsed in dH₂O, dehydrated through ethanol series and mounted with DPX (Sigma).

Bulk RNA sequencing and data analysis

Sample processing and cDNA

Cell sorting and RNA sequencing was performed as previously described (Kuil et al. 2020 [↗](#)). Approximately 8,000 microglial cells (*p2ry12*⁺; *cd45*⁺ or *mhc2dab*⁺; *cd45*^{low}, n=2 for each Tg) and 1,200 DC-like cells (*mhc2dab*⁺; *cd45*^{high}, n=2) were sorted. RNA was isolated using the miRNeasy Micro Kit (Qiagen) according to the manufacturer's instructions. RNA concentration and quality were evaluated using a Bioanalyzer 2100 (Agilent technologies). The Ovation Solo RNA-Seq System (NuGen-TECAN) with the SoLo Custom AnyDeplete Probe Mix (Zebrafish probe set) were used to obtain indexed cDNA libraries following manufacturer recommendation.

Sequencing

Sequencing libraries were loaded on a NovaSeq 6000 (Illumina) using a S2 flow cell and reads/fragments were sequenced using a 200 Cycle Kit.

Alignment and feature counting

Sequenced reads were then trimmed using *cutadapt* with default parameters except for "--overlap 5 --cut 5 --minimum-length 25:25 -e 0.05". Trimmed FQ files were at this point processed with the same approach for both datasets, including Wu et al. 2021 expression data that were retrieved from GEO data repository (GEO Accession: GSM4725741) (Wu et al. 2020 [↗](#)). Trimmed and filtered reads were then mapped against the reference genome GRCz11.95 using STAR aligner with the "--twopassMode basic" and "--sjdbOverhang 100". BAM files were then indexed and filtered using SAMTOOLS "view -b -f 3 -F 256". Finally, transcript feature annotations for Ensembl genes using *Danio rerio* v. GRCz11.95 were quantified using HTSeq-counts call with default parameters

specifying “-r pos -s yes -a 10 --additional-attr=gene_name -m intersection-nonempty --secondary-alignments=ignore --supplementary-alignments=ignore”. General sequencing and mapping stats were calculated using fastqc and multiQC.

Feature count matrix preprocessing, normalization and differential expression

Feature count matrices were further preprocessed filtering low count genes (≥ 10) for 2 out of 2 samples in each group (this manuscript dataset) or 3 out of 5 samples per group (Wu et al. 2020 [↗](#) dataset). Overall, for this manuscript dataset, we obtained 13663 genes expressed in both replicates whereas Wu et al. 2020 [↗](#) dataset, showed 9007 genes that were expressed in at least 3 of the 5 replicates. Then DESeq2 (v. 1.30.0) for R statistical computing was used to normalize the raw counts and perform differential expression analysis focussing on protein-coding genes with de-duplicated gene names (as “_#”) (Love, Huber, and Anders 2014 [↗](#)). Statistical differential expression and downstream analyses were performed using R Statistical software v. 4.0.3.

Single-cell RNA sequencing and data analysis

Single-Cell RNA-seq library preparation and sequencing

Adult brain single-cell suspensions were prepared as described before from adult *Tg(p2ry12:GFP; cd45:DsRed)* fish (n=3), using calcein violet to exclude dead cells (1 μ M, Thermo Fisher). A total of 14,000 *cd45:DsRed*⁺ cells were processed for single-cell profiling using the 10x Genomics platform and diluted to a density of 800 cells/ μ l following 10x Genomics Chromium Single cell 3' kit (v3) instructions. Library preparation was performed according to 10x Genomics guidelines and sequenced on an Illumina NextSeq 550. Raw sequencing data was processed using the Cell Ranger with a custom-built reference based on the zebrafish reference genome GRCz11 and gene annotation Ensembl 92 in which the EGFP and DsRed sequence were included.

Single-cell RNA-seq data preprocessing

Single cell raw counts were processed using Seurat (v3) (Butler et al. 2018 [↗](#); Satija et al. 2015 [↗](#)). Briefly, genes with zero counts for all cells were removed, and applied cell filters for $\geq 20\%$ reads mapping to mitochondrial genes and nFeature >300. Additionally, mitochondrial genes ‘^mt-’ and ribosomal genes ‘^rp[sl]’ were masked for further downstream analysis, as well as non-coding protein genes selected with the current feature annotations of the EnsemblGene 95 from GRCz11 zebrafish genome. Overall, providing a dataset of 4,145 cells and 18,807 genes for single cell data analysis.

Single-Cell Normalization, clustering and marker genes

Filtered cell data was normalized using the SCT transform approach for Seurat using “variable.features.n=4000 and return.only.var.genes=F”. Then, the nearest neighbour graph was build with 40 PCA dimensions, and clusters were identified using manually selected resolution based on the supervised inspection of know markers leading to the optimal “resolution= 0.6 (Louvain)” and “n.neighbors=20”. The same parameters were used for the dimensionality reduction as UMAP. Finally, cluster annotation was performed by inspecting the identified marker genes using FindAllMarkers function (one v. rest with default parameters except for “min.pct=0.25”).

Single Cell Pathway analysis

For pathway analysis, marker genes of all four microglia clusters together (MG1, MG2, MG3, MG4) or all four DC-like clusters (DC1, DC2, DC3, DC4) were obtained using Seurat’s FindMarkers function. Next, differentially expressed zebrafish genes (log2 fold-change >0.25, P-adjusted < 0.05)

were converted to their human orthologs using gProfiler tool (Raudvere et al. 2019) and validated using the ZFIN (zfin.org) and Alliance Genome databases (www.alliancegenome.org). Genes with no corresponding orthologs were not included. From this gene lists, Gene ontology terms (Biological Processes) and Reactome pathways were obtained using the Cytoscape ClueGO application (two-sided hypergeometric statistical test, Bonferroni correction) (Bindea et al. 2009). To explore MG and DC-like conserved cell type signatures (Table 4), each gene list was uploaded to the Enrichr database (Xie et al. 2021) to identify the most enriched “Cell Types” categories querying PanglaoDB (Franzen, Gan, and Bjorkegren 2019).

Quantitative PCR

RNA extraction was performed using the RNeasy Plus Mini kit (Qiagen) and cDNAs were synthesized using the qscript cDNA supermix (Quanta Biosciences), as previously described (Ferrero et al. 2018). Reactions were run on a Bio-Rad CFX96™ real time system (Bio-Rad), using the Kapa SYBR Fast qPCR Master Mix (2X) kit (Kapa Biosystems) under the following thermal cycling conditions: 3 min at 95°C and 40 cycles of 5 s at 95°C, 30 s at 60°C. A final dissociation at 95°C for 10 s and a melting curve from 65 to 95°C (0.5°C increase every 5 s) were included to verify the specificity and absence of primer dimers. Biological replicates were compared for each subset. Relative amount of each transcript was quantified via the ΔCt method, using *elongation-Factor-1-alpha* (*eef1a111*; ENSDARG00000020850) expression for normalization.

Immunostaining and vibratome sections

Adult brains were dissected, fixed in 4% PFA, incubated overnight in 30% sucrose:PBS before snap-freezing in OCT (Tissue-Tek, Leica) and stored at -80°C. Immunostaining was performed on 14 μm cryosections as described (Ferrero et al. 2018). The following primary and secondary antibodies were used: chicken anti-GFP polyclonal antibody (1:500; Abcam, Cat# ab13970), rabbit anti-Lcp1 (1:1000), mouse anti-mCherry monoclonal antibody (1:500; Takara Bio Cat# 632543), Alexa Fluor 488-conjugated anti-chicken IgG antibody (1:500; Abcam Cat# ab150169), Alexa Fluor 594-conjugated anti-rabbit IgG (1:500; Abcam Cat# ab150076), Alexa Fluor 647-conjugated anti-mouse IgG (1:500; Abcam Cat# ab150107). For vibratome sections, adult brains were fixed in 4% PFA and included in 7% low-melting agarose in PBS 1X and sectioned at 100 μm using a vibratome (Leica). Sections were mounted with Glycergel (Dako) and imaged.

Imaging and image analyses

Fluorescent samples were imaged using a Zeiss LSM 780 inverted microscope (Zeiss, Oberkochen, Germany), with a Plan Aplanachromat 20X objective. Image post-processing was performed using Zeiss Zen Software (ZEN Digital Imaging for Light Microscopy), as previously described (Ferrero et al. 2021). Cells were manually counted using the Black Zen software and divided by the area of the brain section (cell density/ μm^2) and quantified between 5-11 transversal sections per brain. Cytospun cells were imaged using a Leica DM 2000 microscope equipped with a 100X objective, and scanned using a NanoZoomer-SQ Digital Slide scanner (Hamamatsu).

Data collection

The sample size was chosen based on previous experience in the laboratory, for each experiment to yield high power to detect specific effects. No statistical methods were used to predetermine sample size and experiments were repeated at least twice. Homozygous mutant animals used in this study were obtained by heterozygous mating. No fish were excluded. Genotyping was performed on tail biopsies collected from individual euthanized fish, in parallel to brain dissection. Randomly selected samples for each genotype were then immunostained in one batch, assessed phenotypically in a blind manner and grouped based on their genotype.

Statistical analyses

Statistical differences between mean values of two experimental groups were analyzed by Student's t-test or the equivalent U-Mann-Whitney non-parametric test, when parametric assumptions were not met in the sample data. Results are expressed as mean \pm standard of the mean (SEM) and considered to be significant at $P < 0.05$. Details on the number of fish (biological replicates) used in each experiment, the statistical test used and statistical significance are indicated in each figure and figure legends. Statistical analyses were performed using GraphPad Prism8.

Acknowledgements

We thank all members of the Wittamer lab and Sumeet Pal Singh for critical discussion and comments on the manuscript. We are also grateful to Marianne Caron for technical assistance and to Daniel M. Borràs for guidance with bioinformatic analyses. We also acknowledge Christine Dubois for support with flow cytometry, F. Libert and A. Lefort from the ULB Genomic Core Facility and S. Reinhardt, A. Kränkel and A. Petzold at the Dresden-Concept Genome center in Germany.

Competing interests

The authors declare no competing financial interests.

Funding

This work was funded in part by the Funds for Scientific Research (FNRS) under Grant Numbers F451218F, UN06119F and UG03019F, the program ARC from the Wallonia-Brussels Federation, the Minerve Foundation (to V.W.), the Fonds David et Alice Van Buuren, the Fondation Jaumotte-Demoulin and the Fondation Héger-Masson (to V.W., G.F. and M.M.). M.R. is supported by a Chargé de Recherche fellowship (FNRS), G.F. and A.M. by a Research Fellowship (FNRS) and M.M. by a fellowship from The Belgian Kid's Fund.

Data availability statement

All datasets and material generated for this study are included in the manuscript/ Supplementary Files and will be shared upon request. Raw data for single cell RNA-seq samples and RNA-seq are available in the ArrayExpress database as accession number E-MTAB-13223 and E-MTAB-13228, respectively.

Antibody	Alexa Fluor 647-conjugated anti-mouse IgG	Abcam	RRID:AB_2890037 1:500
Commercial assay or kit	SP6 RNA Polymerase	New England BioLabs	Cat# M0207
Commercial assay or kit	High Pure PCR Cleanup Microkit	Roche	Cat# 498395500
Commercial assay or kit	Rneasy Plus mini kit	Qiagen	Cat# 74134
Chemical compound, drug	SYTOX™Red	Invitrogen	Cat# S34859
Chemical compound, drug	qScript cDNA SuperMix	Quanta Biosciences	Cat# 95048-100
Software, algorithm	Flow-Jo LLC	TreeStar	RRID:SCR_008520
Software, algorithm	Black Zen software	Zeiss, Germany	RRID:SCR_018163
Software, algorithm	Blue Zen software	Zeiss, Germany	RRID:SCR_013672
Software, algorithm	R Statistical software v. 4.0.3	R Project for Statistical Computing	RRID:SCR_001905
Software, algorithm	GraphPad Prism 8	GraphPad software, USA	RRID:SCR_002798

References

- Alestrom P., D'Angelo L., Midtlyng P. J., Schorderet D. F., Schulte-Merker S., Sohm F., Warner S. (2019) **'Zebrafish: Housing and husbandry recommendations'** *Lab Anim*
- Alves de Lima K. *et al.* (2020) **Meningeal gammadelta T cells regulate anxiety-like behavior via IL-17a signaling in neurons** *Nat Immunol* **21**:1421–29
- Bassity E., Clark T. G. (2012) **Functional identification of dendritic cells in the teleost model, rainbow trout (*Oncorhynchus mykiss*)** *PLoS One* **7**
- Bindea G., Mlecnik B., Hackl H., Charoentong P., Tosolini M., Kirilovsky A., Fridman W. H., Pages F., Trajanoski Z., Galon J. (2009) **ClueGO: a Cytoscape plug-in to decipher functionally grouped gene ontology and pathway annotation networks** *Bioinformatics* **25**:1091–3
- Bjorklund A. K., Forkel M., Picelli S., Konya V., Theorell J., Friberg D., Sandberg R., Mjosberg J. (2016) **The heterogeneity of human CD127(+) innate lymphoid cells revealed by single-cell RNA sequencing** *Nat Immunol* **17**:451–60
- Bottcher C. *et al.* (2019) **Human microglia regional heterogeneity and phenotypes determined by multiplexed single-cell mass cytometry** *Nat Neurosci* **22**:78–90
- Butler A., Hoffman P., Smibert P., Papalexi E., Satija R. (2018) **Integrating single-cell transcriptomic data across different conditions, technologies, and species** *Nat Biotechnol* **36**:411–20
- Butovsky O. *et al.* (2014) **Identification of a unique TGF-beta-dependent molecular and functional signature in microglia** *Nat Neurosci* **17**:131–43
- Butovsky O., Weiner H. L. (2018) **Microglial signatures and their role in health and disease** *Nat Rev Neurosci* **19**:622–35
- Cabeza-Cabrerizo M., Cardoso A., Minutti C. M., Pereira da Costa M., Sousa E., Reis C. (2021) **Dendritic Cells Revisited** *Annu Rev Immunol* **39**:131–66
- Carmona S. J., Teichmann S. A., Ferreira L., Macaulay I. C., Stubbington M. J., Cvejic A., Gfeller D. (2017) **Single-cell transcriptome analysis of fish immune cells provides insight into the evolution of vertebrate immune cell types** *Genome Res* **27**:451–61
- Croese T., Castellani G., Schwartz M. (2021) **Immune cell compartmentalization for brain surveillance and protection** *Nat Immunol* **22**:1083–92
- D'Amora M., Galgani A., Marchese M., Tantussi F., Faraguna U., De Angelis F., Giorgi F. S. (2023) **'Zebrafish as an Innovative Tool for Epilepsy Modeling: State of the Art and Potential Future Directions'** *Int J Mol Sci* **24**
- Dee C. T., Nagaraju R. T., Athanasiadis E. I., Gray C., Fernandez Del Ama L., Johnston S. A., Secombes C. J., Cvejic A., Hurlstone A. F. (2016) **CD4-Transgenic Zebrafish Reveal Tissue-Resident Th2- and Regulatory T Cell-like Populations and Diverse Mononuclear Phagocytes** *J Immunol* **197**:3520–30

Drieu A. *et al.* (2022) **'Parenchymal border macrophages regulate the flow dynamics of the cerebrospinal fluid'** *Nature* **611**:585–93

Earley A. M., Graves C. L., Shiao C. E. (2018) **Critical Role for a Subset of Intestinal Macrophages in Shaping Gut Microbiota in Adult Zebrafish** *Cell Rep* **25**:424–36

Ellett F., Pase L., Hayman J. W., Andrianopoulos A., Lieschke G. J. (2010) **mpeg1 promoter transgenes direct macrophage-lineage expression in zebrafish** *Blood* **117**:e49–56

Ferrero G., Gomez E., Lyer S., Rovira M., Miserocchi M., Langenau D. M., Bertrand J. Y., Wittamer V. (2020) **The macrophage-expressed gene (mpeg) 1 identifies a subpopulation of B cells in the adult zebrafish** *J Leukoc Biol* **107**:431–43

Ferrero G. *et al.* (2018) **Embryonic Microglia Derive from Primitive Macrophages and Are Replaced by cmyb-Dependent Definitive Microglia in Zebrafish** *Cell Rep* **24**:130–41

Ferrero G., Miserocchi M., Di Ruggiero E., Wittamer V. (2021) **A csf1rb mutation uncouples two waves of microglia development in zebrafish** *Development*

Franzen O., Gan L. M., Bjorkegren J. L. M. (2019) **PanglaoDB: a web server for exploration of mouse and human single-cell RNA sequencing data** *Database (Oxford)* **2019**

Gerrits E., Heng Y., Boddeke Ewgm, Eggen B. J. L. (2020) **Transcriptional profiling of microglia; current state of the art and future perspectives** *Glia* **68**:740–55

Hammond T. R. *et al.* (2018) **Single-Cell RNA Sequencing of Microglia throughout the Mouse Lifespan and in the Injured Brain Reveals Complex Cell-State Changes** *Immunity*

Hason M., Mikulasova T., Machonova O., Pombinho A., van Ham T. J., Irion U., Nusslein-Volhard C., Bartunek P., Svoboda O. (2022) **M-CSFR/CSF1R signaling regulates myeloid fates in zebrafish via distinct action of its receptors and ligands** *Blood Adv* **6**:1474–88

Herbomel P., Thisse B., Thisse C. (2001) **Zebrafish early macrophages colonize cephalic mesenchyme and developing brain, retina, and epidermis through a M-CSF receptor-dependent invasive process** *Dev Biol* **238**:274–88

Hernández P. P., Strzelecka P. M., Athanasiadis E. I., Dominic Hall D., Robalo A. F., Collins C. M., Boudinot P., Levraud J. P., Cvejic A. (2018) **Single-cell transcriptional analysis reveals ILC-like cells in zebrafish** *Sci. Immunol* **3**

Jordao M. J. C. *et al.* (2019) **Single-cell profiling identifies myeloid cell subsets with distinct fates during neuroinflammation** *Science* **363**

Jurga A. M., Paleczna M., Kuter K. Z. (2020) **Overview of General and Discriminating Markers of Differential Microglia Phenotypes** *Front Cell Neurosci* **14**

Kaunzner U. W., Miller M. M., Gottfried-Blackmore A., Gal-Toth J., Felger J. C., McEwen B. S., Bulloch K. (2012) **Accumulation of resident and peripheral dendritic cells in the aging CNS** *Neurobiol Aging* **33**:681–93

Kizil C., Kyritsis N., Dudczig S., Kroehne V., Freudenreich D., Kaslin J., Brand M. (2012) **Regenerative neurogenesis from neural progenitor cells requires injury-induced expression of Gata3** *Dev Cell* **23**:1230–7

- Kuil L. E. *et al.* (2020) **Zebrafish macrophage developmental arrest underlies depletion of microglia and reveals Csf1r-independent metaphocytes** *Elife* **9**
- Kuil L. E., Oosterhof N., Geurts S. N., van der Linde H. C., Meijering E., van Ham T. J. (2019) **Reverse genetic screen reveals that IL34 facilitates yolk sac macrophage distribution and seeding of the brain** *Dis Model Mech* **12**
- Kyritsis N., Kizil C., Zocher S., Kroehne V., Kaslin J., Freudenreich D., Iltzsche A., Brand M. (2012) **Acute inflammation initiates the regenerative response in the adult zebrafish brain** *Science* **338**:1353–6
- Langenau D. M., Ferrando A. A., Traver D., Kutok J. L., Hezel J. P., Kanki J. P., Zon L. I., Look A. T., Trede N. S. (2004) **In vivo tracking of T cell development, ablation, and engraftment in transgenic zebrafish** *Proc Natl Acad Sci U S A* **101**:7369–74
- Lewis K. L., Del Cid N., Traver D. (2014) **Perspectives on antigen presenting cells in zebrafish** *Dev Comp Immunol* **46**:63–73
- Liu Y (2023) **Zebrafish as a Model Organism for Studying Pathologic Mechanisms of Neurodegenerative Diseases and other Neural Disorders** *Cell Mol Neurobiol* **43**:2603–20
- Love M. I., Huber W., Anders S. (2014) **Moderated estimation of fold change and dispersion for RNA-seq data with DESeq2** *Genome Biol* **15**
- Ludewig P., Gallizioli M., Urra X., Behr S., Brait V. H., Gelderblom M., Magnus T., Planas A. M. (2016) **Dendritic cells in brain diseases** *Biochim Biophys Acta* **1862**:352–67
- Lugo-Villarino G., Balla K. M., Stachura D. L., Banuelos K., Werneck M. B., Traver D. (2010) **Identification of dendritic antigen-presenting cells in the zebrafish** *Proc Natl Acad Sci U S A* **107**:15850–5
- Maddaluno L., Verbrugge S. E., Martinoli C., Matteoli G., Chiavelli A., Zeng Y., Williams E. D., Rescigno M., Cavallaro U. (2009) **The adhesion molecule L1 regulates transendothelial migration and trafficking of dendritic cells** *J Exp Med* **206**:623–35
- Masuda T. *et al.* (2019) **Spatial and temporal heterogeneity of mouse and human microglia at single-cell resolution** *Nature* **566**:388–92
- Masuda Takahiro, Sankowski Roman, Staszewski Ori, Prinz Marco (2020) **Microglia Heterogeneity in the Single-Cell Era** *Cell Reports* **30**:1271–81
- Mathias J. R., Walters K. B., Huttenlocher A. (2009) **Neutrophil motility in vivo using zebrafish** *Methods Mol Biol* **571**:151–66
- Mazzolini J., Le Clerc S., Morisse G., Coulonges C., Kuil L. E., van Ham T. J., Zagury J. F., Sieger D. (2019) **Gene expression profiling reveals a conserved microglia signature in larval zebrafish** *Glia*
- Milner J. J. *et al.* (2017) **Runx3 programs CD8(+) T cell residency in non-lymphoid tissues and tumours** *Nature* **552**:253–57
- Minhas Paras S. *et al.* (2021) **Restoring metabolism of myeloid cells reverses cognitive decline in ageing** *Nature*

- Moore F. E. *et al.* (2016) **Single-cell transcriptional analysis of normal, aberrant, and malignant hematopoiesis in zebrafish** *J Exp Med* **213**:979–92
- Moyse B. R., Richardson R. J. (2020) **A Population of Injury-Responsive Lymphoid Cells Expresses mpeg1.1 in the Adult Zebrafish Heart** *Immunohorizons* **4**:464–74
- Mrdjen D. *et al.* (2018) **High-Dimensional Single-Cell Mapping of Central Nervous System Immune Cells Reveals Distinct Myeloid Subsets in Health, Aging, and Disease** *Immunity* **48**:380–95
- Mundt S., Greter M., Flugel A., Becher B. (2019) **The CNS Immune Landscape from the Viewpoint of a T Cell** *Trends Neurosci* **42**:667–79
- Oosterhof N., Kuil L. E., van der Linde H. C., Burm S. M., Berdowski W., van Ijcken W. F. J., van Swieten J. C., Hol E. M., Verheijen M. H. G., van Ham T. J. (2018) **Colony-Stimulating Factor 1 Receptor (CSF1R) Regulates Microglia Density and Distribution, but Not Microglia Differentiation In Vivo** *Cell Rep* **24**:1203–17
- Page D. M. *et al.* (2013) **An evolutionarily conserved program of B-cell development and activation in zebrafish** *Blood* **122**:e1–11
- Parichy DM, Ransom DG, Paw B, Zon LI, Johnson SL (2000) **An orthologue of the kit-related gene *fms* is required for development of neural crest-derived xanthophores and a subpopulation of adult melanocytes in the zebrafish, *Danio rerio*** *Development* **127**:3031–44
- Pasciuto E. *et al.* (2020) **Microglia Require CD4 T Cells to Complete the Fetal-to-Adult Transition** *Cell* **182**:625–40
- Peri F., Nusslein-Volhard C. (2008) **Live imaging of neuronal degradation by microglia reveals a role for v0-ATPase a1 in phagosomal fusion in vivo** *Cell* **133**:916–27
- Raudvere U., Kolberg L., Kuzmin I., Arak T., Adler P., Peterson H., Vilo J. (2019) **g:Profiler: a web server for functional enrichment analysis and conversions of gene lists (2019 update)** *Nucleic Acids Res* **47**:W191–W98
- Rovira M., Miserocchi M., Montanari A., Hammou L., Chomette L., Pozo J., Imbault V., Bisteau X., Wittamer V. (2022) **Zebrafish Galectin 3 binding protein is the target antigen of the microglial 4C4 monoclonal antibody** *Dev Dyn*
- Saraswathy V. M., Zhou L., McAdow A. R., Burriss B., Dogra D., Reischauer S., Mokalled M. H. (2022) **Myostatin is a negative regulator of adult neurogenesis after spinal cord injury in zebrafish** *Cell Rep* **41**
- Satija R., Farrell J. A., Gennert D., Schier A. F., Regev A. (2015) **Spatial reconstruction of single-cell gene expression data** *Nat Biotechnol* **33**:495–502
- Shiau C. E., Kaufman Z., Meireles A. M., Talbot W. S. (2015) **Differential requirement for *irf8* in formation of embryonic and adult macrophages in zebrafish** *PLoS One* **10**
- Sieger D., Moritz C., Ziegenhals T., Prykhodzij S., Peri F. (2012) **Long-range Ca²⁺ waves transmit brain-damage signals to microglia** *Dev Cell* **22**:1138–48

- Silva N. J., Dorman L. C., Vainchtein I. D., Horneck N. C., Molofsky A. V. (2021) **In situ and transcriptomic identification of microglia in synapse-rich regions of the developing zebrafish brain** *Nat Commun* **12**
- Spits H., Cupedo T. (2012) **Innate lymphoid cells: emerging insights in development, lineage relationships, and function** *Annu Rev Immunol* **30**:647–75
- Stratoulas V., Venero J. L., Tremblay M. E., Joseph B. (2019) **Microglial subtypes: diversity within the microglial community** *EMBO J*
- Talbot J. C., Amacher S. L. (2014) **A streamlined CRISPR pipeline to reliably generate zebrafish frameshifting alleles** *Zebrafish* **11**:583–5
- Tanabe S., Yamashita T. (2018) **B-1a lymphocytes promote oligodendrogenesis during brain development** *Nat Neurosci* **21**:506–16
- Tang Q. *et al.* (2014) **Optimized cell transplantation using adult rag2 mutant zebrafish** *Nat Methods* **11**:821–4
- Tang Q. *et al.* (2017) **Dissecting hematopoietic and renal cell heterogeneity in adult zebrafish at single-cell resolution using RNA sequencing** *J Exp Med* **214**:2875–87
- Turrini L., Roschi L., de Vito G., Pavone F. S., Vanzi F. (2023) **Imaging Approaches to Investigate Pathophysiological Mechanisms of Brain Disease in Zebrafish** *Int J Mol Sci* **24**
- Van Hove H. *et al.* (2019) **A single-cell atlas of mouse brain macrophages reveals unique transcriptional identities shaped by ontogeny and tissue environment** *Nat Neurosci* **22**:1021–35
- Vivier E. *et al.* (2018) **Innate Lymphoid Cells: 10 Years On** *Cell* **174**:1054–66
- Vivier E., van de Pavert S. A., Cooper M. D., Belz G. T. (2016) **The evolution of innate lymphoid cells** *Nat Immunol* **17**:790–4
- Wittamer V., Bertrand J. Y., Gutschow P. W., Traver D. (2011) **Characterization of the mononuclear phagocyte system in zebrafish** *Blood* **117**:7126–35
- Wong S. H. *et al.* (2012) **Transcription factor RORalpha is critical for nuocyte development** *Nat Immunol* **13**:229–36
- Wu S., Nguyen L. T. M., Pan H., Hassan S., Dai Y., Xu J., Wen Z. (2020) **Two phenotypically and functionally distinct microglial populations in adult zebrafish** *Science Advances*
- Wu S. Y., Shin J., Sepich D. S., Solnica-Krezel L. (2012) **Chemokine GPCR signaling inhibits beta-catenin during zebrafish axis formation** *PLoS Biol* **10**
- Xie Z. *et al.* (2021) . **'Gene Set Knowledge Discovery with Enrichr'** *Curr Protoc* **1**
- Xu H. *et al.* (2015) **Sequence determinants of improved CRISPR sgRNA design** *Genome Res* **25**:1147–57
- Yanez A., Goodridge H. S. (2016) **Interferon regulatory factor 8 and the regulation of neutrophil, monocyte, and dendritic cell production** *Curr Opin Hematol* **23**:11–7

Yoder J. A., Turner P. M., Wright P. D., Wittamer V., Bertrand J. Y., Traver D., Litman G. W. (2010) **Developmental and tissue-specific expression of NITRs** *Immunogenetics* **62**:117–22

Zambusi A. *et al.* (2022) **TDP-43 condensates and lipid droplets regulate the reactivity of microglia and regeneration after traumatic brain injury** *Nat Neurosci* **25**:1608–25

Article and author information

Mireia Rovira

Institut de Recherche Interdisciplinaire en Biologie Humaine et Moléculaire (IRIBHM), ULB Institute of Neuroscience (UNI), Université Libre de Bruxelles (ULB), Brussels, Belgium
ORCID iD: [0000-0003-4050-1662](https://orcid.org/0000-0003-4050-1662)

Giuliano Ferrero

Institut de Recherche Interdisciplinaire en Biologie Humaine et Moléculaire (IRIBHM), ULB Institute of Neuroscience (UNI), Université Libre de Bruxelles (ULB), Brussels, Belgium
ORCID iD: [0000-0001-5382-9873](https://orcid.org/0000-0001-5382-9873)

Magali Miserocchi

Institut de Recherche Interdisciplinaire en Biologie Humaine et Moléculaire (IRIBHM), ULB Institute of Neuroscience (UNI), Université Libre de Bruxelles (ULB), Brussels, Belgium
ORCID iD: [0000-0002-4120-5833](https://orcid.org/0000-0002-4120-5833)

Alice Montanari

Institut de Recherche Interdisciplinaire en Biologie Humaine et Moléculaire (IRIBHM), ULB Institute of Neuroscience (UNI), Université Libre de Bruxelles (ULB), Brussels, Belgium
ORCID iD: [0000-0003-2863-4761](https://orcid.org/0000-0003-2863-4761)

Valérie Wittamer

Institut de Recherche Interdisciplinaire en Biologie Humaine et Moléculaire (IRIBHM), ULB Institute of Neuroscience (UNI), Université Libre de Bruxelles (ULB), Brussels, Belgium
For correspondence: valerie.wittamer@ulb.be
ORCID iD: [0000-0003-0003-2646](https://orcid.org/0000-0003-0003-2646)

Copyright

© 2024, Rovira et al.

This article is distributed under the terms of the [Creative Commons Attribution License](https://creativecommons.org/licenses/by/4.0/), which permits unrestricted use and redistribution provided that the original author and source are credited.

Editors

Reviewing Editor

Jean-Pierre Levrud

Institut Pasteur, Paris, France

Senior Editor

Didier Stainier

Max Planck Institute for Heart and Lung Research, Bad Nauheim, Germany

Reviewer #1 (Public Review):

Summary:

The authors used several zebrafish reporter lines to demonstrate the presence, regional distribution, and transcriptional profile of the immune cells in adult zebrafish brains. They identified DC-like cells distinct from microglia or other macrophages, resembling murine cDC1s. Analysis of different mutants further revealed that this DC population was dependent on *Irf8*, *Batf3*, and *Csf1rb*, but did not rely on *Csf1ra*.

Strengths:

It is an elegantly designed study providing compelling evidence for further heterogeneity among brain mononuclear phagocytes in zebrafish, consisting of microglia, macrophages, and DC-like cells. This will provide a better understanding of the immune landscape in the zebrafish brain and will help to better distinguish the different cell types from microglia, and to assign specific functions.

Weaknesses:

While scRNA-seq data clearly revealed different subsets of microglia, macrophages, and DCs in the brain, it remains somewhat challenging to distinguish DC-like cells from P2ry12-macrophages by immunohistochemistry or flow cytometry.

- <https://doi.org/10.7554/eLife.91427.1.sa2>

Reviewer #2 (Public Review):

The authors made an atlas of single-cell transcriptome of on a pure population of leukocytes isolated from the brain of adult Tg(*cd45:DsRed*) transgenic animals by flow cytometry. Seven major leukocyte populations were identified, comprising microglia, macrophages, dendritic-like cells, T cells, natural killer cells, innate lymphoid-like cells, and neutrophils. Each cluster was analyzed to characterize subclusters. Among lymphocytes, in addition to 2 subclusters expressing typical T cell markers, a group of *il4+* *il13+* *gata3+* cells was identified as possible ILC2. This hypothesis is supported by the presence of this population in *rag2KO* fish, in which the frequency of *lck* and *zap70+* cells is strongly reduced. The use of KO lines for such validations is a strength of this work (and the zebrafish model).

The subcluster analysis of *mpeg1.1* + myeloid cells identified 4 groups of microglial cells, one novel group of macrophage-like cells (expressing *s100a10b*, *sftpb*, *icn*, *fthl27*, *anxa5b*, *f13a1b* and *spi1b*), and several groups of DC like cells expressing the markers *siglec15l*, *ccl19a.1*, *ccr7*, *id2a*, *xcr1a.1*, *batf3*, *flt3*, *chl1a* and *hepacam2*. Combining these new markers and transgenic reporter fish lines, the authors then clarified the location of leukocyte subsets within the brain, showing for example that DC-like cells stand as a parenchymal population along with microglia. Reporter lines were also used to perform a detailed analysis of cell subsets, and cross with a *batf3* mutant demonstrated that DC-like cells are *batf3* dependent, which was similar to mouse and human cDC1. Finally, analysis of classical mononuclear phagocyte deficient zebrafish lines showed they have reduced numbers of microglia but exhibit distinct DC-like cell phenotypes. A weakness of this study is that it is mainly based on FACS sorting, which might modify the proportion of different subtypes.

This atlas of zebrafish brain leukocytes is an important new resource for scientists using the zebrafish models for neurology, immunology, and infectiology, and for those interested in the evolution of the brain and immune system.

- <https://doi.org/10.7554/eLife.91427.1.sa1>

Reviewer #3 (Public Review):

Rovira, et al., aim to characterize immune cells in the brain parenchyma and identify a novel macrophage population referred to as "dendritic-like cells". They use a combination of single-cell transcriptomics, immunohistochemistry, and genetic mutants to conclude the presence of this "dendritic-like cell" population in the brain. The strength of this manuscript is the identification of dendritic cells in the brain, which are typically found in the meningeal layers and choroid plexus. A weakness is the lack of specific reporters or labeling of this dendritic cell population using specific genes found in their single-cell dataset. Additionally, it is difficult to remove the meningeal layers from the brain samples and thus can lead to confounding conclusions. Overall, I believe this study should be accepted contingent on sufficient labeling of this population and addressing comments.

- <https://doi.org/10.7554/eLife.91427.1.sa0>